Missouri S&T Library and Learning Resources

Scholars' Mine

Masters Theses Student Theses and Dissertations

Spring 2016

Measurements and simulation of conductor-related loss of PCB transmission lines

Oleg Kashurkin

Follow this and additional works at: https://scholarsmine.mst.edu/masters_theses

Part of the Electrical and Computer Engineering Commons

Department:

Recommended Citation

Kashurkin, Oleg, "Measurements and simulation of conductor-related loss of PCB transmission lines" (2016). *Masters Theses*. 7508.
https://scholarsmine.mst.edu/masters_theses/7508

This thesis is brought to you by Scholars' Mine, a service of the Missouri S&T Library and Learning Resources. This work is protected by U. S. Copyright Law. Unauthorized use including reproduction for redistribution requires the permission of the copyright holder. For more information, please contact scholarsmine@mst.edu.

MEASUREMENTS AND SIMULATION OF CONDUCTOR-RELATED LOSS OF PCB TRANSMISSION LINES

by

OLEG KASHURKIN

A THESIS

Presented to the Faculty of the Graduate School of the

MISSOURI UNIVERSITY OF SCIENCE AND TECHNOLOGY

In Partial Fulfillment of the Requirements for the Degree

MASTER OF SCIENCE IN ELECTRICAL ENGINEERING

2016

Approved by

Victor Khilkevich, Advisor
David Pommerenke
Jun Fan

© 2016
Oleg Kashurkin
All Rights Reserved

ABSTRACT

With continuously increasing data rates Signal Integrity (SI) problems become more and more challenging. One of the main issues in high-speed data transfer is the frequency-dependent loss of transmission lines. This thesis is dedicated to conductor-related loss mechanisms in printed circuit board (PCB) transmission lines.

This thesis provides the experimental investigation of conductor properties used for fabrication of PCBs. Particularly, the resistivity and conductivity along with the temperature coefficients of eleven copper types is measured and reported. A four probe measurement technique is used. Results were verified by two independent measurements and show discrepancy of less than 0.5%.

Another major conductor-related loss mechanism is the attenuation of the electromagnetic waves due to the surface roughness of PCB conductors. There are several models attempting to take into account the roughness effect. However none of them are able to explain or predict the transmission line behavior with high accuracy. Particularly, the experimental observations show that the slope of S_{21} curves increases with frequency, which cannot be modelled by the existing model. To better understand the physics associated with the loss due to the surface roughness of conductors, and be able to predict the behavior of transmission lines in the future, a full wave model of surface roughness was developed. The detailed methodology for 3D roughness generation is provided.

ACKNOWLEDGMENTS

I would like to express my sincere gratitude and deep appreciation to my advisor, Dr. Victor Khilkevich for guidance toward my academic path, ideas and help with experiment conducting technique. I am very thankful him for introduction to real world electrical engineering, revel modern and challenge problems of high-speed design and EMC. I express my sincere gratitude to Dr. Marina Y. Koledintseva, for her constant support and inspiration for work. I thank Dr. James L. Drewniak for his mentoring and guidance in my career and manage project I was involved in as part of the EMC Laboratory and for giving me this opportunity to be a member of EMC lab. I am very grateful to Mr. Scott Hinaga from Cisco Systems, Inc. for his encouragement, attention to new ideas and techniques, and exceptional help throughout my project work.

I want to show my deep gratitude to all professors of the EMC Laboratory for giving me priceless knowledge during course work and showing faith in me as a graduate student. I greatly appreciate classes of Dr. David Pommerenke and Dr. Jun Fan which straightened my understanding of Electromagnetics and Wave propagation Theory. I thank all my fellow laboratory students, who gave me advice and helped me to go through any problems I encountered.

Finally, I would like to thank my beloved family, especially my wife Tatiana Platova for her endless and unconditional love, support, and encouragement through all my education and life.

This thesis is based upon work supported partially by the National Science Foundation under Grant No. IIP-1440110

TABLE OF CONTENTS

Page

ABSTRACT iii

ACKNOWLEDGMENTS iv

LIST OF ILLUSTRATIONS vii

LIST OF TABLES ix

NOMENCLATURE x

SECTION

1. INTRODUCTION 1

1.1. CONDUCTOR – RELATED LOSS IN TRANSMISSION LINE 2

2. MEASUREMENT OF COPPER RESISTIVITY 6

2.1. BACKGROUND 6

2.1.1. Four-Probe Technique 8

2.1.2. Setup 9

2.1.3. DUT Description 12

2.1.4. Uncertainty Estimation 13

2.1.5. Results and Discussion 15

2.2.SUMMARY 21

3. SURFACE ROUGHNESS MODELING 22

3.1. EXPERIMENTAL INVESTIGATION OF SURFACE ROUGHNESS EFFECTS 22

3.1.1. Measurement Results and Observations 23

3.1.2. Motivation and Objective 27

3.2. EXISTING MODELS FOR SURFACE ROUGHNESS 27

3.2.1. Hammerstad Model 27

3.2.2. Hemispherical Model 30

3.2.3. Snowball Model 32

3.2.4. Small Pertrubation Method 34

3.2.5. Scalar Wave Modeling 36

3.2.6. Limitations of Existing Models 36

3.3. 3D MODEL FOR SURFACE ROUGHNESS 37

3.3.1. Extraction of Roughness Parameters 37

3.3.2. Generation of the 3D Surface 40

3.3.3. Surface Roughness Modeling in CST Microwave Studio 46

3.3.4. Results and Discussion 48

4. CONCLUSION 54

BIBLIOGRAPHY 55

VITA 60

LIST OF ILLUSTRATIONS

Figure Page

1.1. Modeled transmission coefficients of stripline at 25 ℃ and 125 ℃ 4

1.2. Optical microscopic images of roughness. From left to right: STD (standard), VLP (very low profile), HVLP (hyper very low profile) 5

1.3. Hall Hemispherical model used in ADS [5] (a), GMS model developed in Simberian Inc. [11] (b) 5

2.1. Schematic of Four - Point Probe Technique 8

2.2. Pogo pin (left), Customized probes for resistivity measurements (right) 9

2.3. Setup schematic for resistance measurements 10

2.4. Setup for resistance measurements (a), window for probes landing (b), two thermocouples placed on the DUT (c) 11

2.5. Top layer of tested coupon 12

2.6. The cross section of the tested trace 13

2.7. Allesi C4S 4-point probe 16

2.8. Conductivity over temperature for all tested copper types 19

2.9. Resistivity over temperature for all tested copper types 19

2.10. Resistivity vs. temperature 20

3.1. Picture of the test vehicle 22

3.2. Drawing of SMA connector 23

3.3. |S21| per inch for the entire PCBs set 24

3.4. Nonlinear behavior of the insertion loss due to the surface roughness [29] 25

3.5. Measured of the real and imaginary components of Roger 5880 [33] 26

3.6. DK, DF of bismaleimide triazine (BT) [47] 26

3.7. Hammersted model for roughness modeling 28

3.8. Roughness correction factor based on Hammersted model 29

3.9. Measured and corrected according to Hammersted insertion loss [5] 29

3.10. Hemispherical model for roughness modeling 31

3.11. Roughness correction factor based on Hemispherical model 31

3.12. Measured and corrected according to Hall insertion loss [5] 32

3.13. Snowballs model for roughness modeling [36] 32

3.14. Roughness correction factor based on Snowballs model..33

3.15. Measured and corrected according to Snowball model insertion loss [5] 34

3.16. Roughness correction factor based on SPM2 35

3.17. Measured and modeled according to SPM2 [39]..35

3.18. Roughness correction factor calculated by SWM vs. SPM2 [43] 36

3.19. Prepared sample for cross section analysis (a), microscopic pictures of stripline (b), close-up picture of the trace (c)..38

3.20. Binary image of the cross-section for VLP...38

3.21. Extracted roughness profile of VLP foil (oxide side)..39

3.22. Autocorrelation function of the VLP foil roughness profile. Correlation length is indicated by the marker...39

3.23. Histogram of VLP foil 40

3.24. Frequency response of a 1D FIR prototype filter 41

3.25. Frequency responses for Wn=0.1, (right) and Wn=0.8 (left). N=4 in both cases.....42

3.26. Surface roughness profile measured by a profilometer [5] (left) and generated (right) 43

3.27. Autocorrelation function of δ-correlated sequence..43

3.28. Measured and generated profiles of the surface roughness with dx=l_{ACR} (1.3μm)...44

3.29. Measured and generated profiles of the surface roughness, with dx=$l_{ACR}/10$ (0.13μm)...45

3.30. Stripline structure to model the surface roughness 47

3.31. Boundary condition and planes of symmetry used for simulation. Blue – magnetic walls, green – electric walls 47

3.32. Zoom of the end of the trace with surface roughness 47

3.33. Five different realization of surface with same parameters 49

3.34. Modeled (a) and measured (b) insertion loss for different roughness magnitude up to 10 GHz...49

3.35. Modeled insertion loss for different roughness magnitude up to 50GHz.................50

3.36. Modeled return loss for different roughness magnitude up to 50GHz 51

3.37. Absorption losses for striplines different roughness magnitude up to 50GHz 51

3.38. Modeled insertion loss for different length of stripline 52

3.39. Modeled return loss for different length of stripline...52

3.40. Absorption losses for striplines of different length up to 50GHz 53

LIST OF TABLES

Table Page

2.1. Values for the electrical resistivity and temperature coefficients of annealed copper 7

2.2. Thickness, width and area of traces 14

2.3. Comparison of conductivity obtained by two methods (3 copper types are shown) 16

2.4. Conductivity at room temperature, 50 ℃ and 100 ℃ 17

2.5. Resistivity at room temperature, 50 ℃ and 100 ℃ 18

2.6. Temperature coefficients for tested copper foils 20

3.1. Roughness parameters for three tested foil types [47] 23

3.2. Difference in loss for different trace width at 15GHz 24

3.3. Filter parameters for two discretization steps 44

3.4. Tetrahedrons and time required for different discretization step 48

NOMENCLATURE

Symbol	Description
$\mathbf{E}$	Electric field vector
E_0	Electromagnetic wave amplitude
ω	Angular frequency
f	Frequency
k	Wave number
γ	Propagation constant
α	Total attenuation constant
β	Phase constant
α_c	Conductor loss
α_d	Dielectric loss
δ	Skin depth
σ	Conductivity of metal
μ	Absolute permeability
ε	Absolute permittivity
ρ	Resistivity
ρ_0	Resistivity at reference temperature
T_0	Reference temperature
α_T	Temperature coefficient
h_{rms}	"root-mean-squared" (RMS) value of surface roughness magnitude
J	Current density

I	Current
A	Cross section area of the trace
x_{μ}	Mean value of sequence
R	Resistance
S	Standard deviation
Δu	Standard uncertainty
$\Delta\rho$	Uncertainty in resistivity
K_s	Power loss coefficient
$\mathrm{A_{tile}}$	Title area
A_{base}	Base area of the hemispheres
$\mathrm{W(k_x, k_y)}$	Power spectral frequency function
l_{ACR}	Correlation length
W_n	Normalized cut-off frequency
G	Gain of the FIR filter

1. INTRODUCTION

The complexity of design and rapidly increasing data rate in high-speed digital electronics makes the signal integrity performance hard to maintain. As the data rate increases the loss in transmission lines becomes the main issue for signals with clock higher than 1GHz [1]. As a signal propagates along a transmission line, the frequency dependent loss causes the signal degradation as the high-frequency part of the spectrum experiences higher attenuation. A transmission line with high loss causes more signal distortion and limits the speed of the transmitted data. This makes it important to determine the high-frequency loss behavior in PCBs at the design stage.

There are several mechanisms of loss in transmission lines but the primary ones are conductor loss, dielectric loss and loss due to the surface roughness of the traces [1] Models of transmission lines need to take into account all three physical loss mechanisms. The conductor and dielectric loss are relatively well studied and good models for them exist [2]. In order to use these models the parameters of materials need to be determined by measurement. The conductor loss is equally important as the dielectric loss, but it is typical to use nominal value for the resistivity of copper to model PCB transmission lines [1, 2]. In this work a practical and easy-to-implement method for the conductor loss measurement (including temperature dependency) is presented. The obtained results indicate that the actual resistivity of copper used to create PCB interconnects is noticeably lower than the nominal value, and needs to be measured in order to improve the accuracy of the transmission line modeling.

Another very important factor determining the loss of PCB transmission lines is the surface roughness of copper layers [3][4]. Despite its importance there is still no satisfactory understanding of physical mechanisms responsible for the roughness-related attenuation and existing models do not provide enough accuracy in many cases as will be shown further. In this work a new full-wave model of conductor surface roughness is proposed, that can be used to investigate physical effect associated with conductor surface roughness.

1.1. CONDUCTOR – RELATED LOSS IN TRANSMISSION LINE

An electromagnetic wave propagating inside any real physical medium experiences attenuation or, in other words, such medium has loss. The attenuation is characterized by attenuation constant and is related to the material properties of the particular medium. The electric field of the x-polarized TEM plane wave propagating along z coordinate is [6]

$$\mathbf{E}(z) = E_0 e^{-\gamma \mathrm{z}} e^{\omega \mathrm{t}} \mathbf{x}, \quad (1)$$

where E_0 is the wave amplitude, ω is the angular frequency, **x** is the unit vector in *x* direction, and γ is a propagation constant given as

$$\gamma = \alpha + j\beta, \quad (2)$$

where α is attenuation constant and β is the phase constant which determines the wave speed in medium it propagates in. Usually, waveguide structures consist of conductor and dielectric both contributing to the attenuation constant. In such structures, the propagating electromagnetic wave is attenuated mainly due to the conductor and dielectric loss, but other factors such as conductor surface roughness are also relevant [5]. For low-loss transmission lines it is possible to separate the total attenuation into a conductor loss and dielectric loss components [1] [2].

$$\alpha \approx \alpha_c + \alpha_d \quad (3)$$

Conductor loss α_c is related to the skin depth $\alpha_c \propto 1/\delta$ which is defined as the depth where the amplitude of the field vectors decays e times. In good conductor the skin depth is [1][3]

$$\delta \approx \sqrt{\frac{1}{f\sigma\pi\mu}}, \quad (4)$$

where f is the frequency, σ is the electrical conductivity and μ is the permeability of the conductor. The electrical conductivity is reciprocal to the electrical resistivity $\sigma = 1/\rho$, and measures a material's ability to conduct an electric current.

The skin effect describes the tendency of alternating current (AC) to flow near the conductor surface. The direct current (DC) distributes uniformly within the entire cross section of the conductor and the resistive loss in this case relates to the cross-section area of the conductor and metal conductivity, but as the frequency increases the current begins to flow in a thin layer beneath the surface of conductor approximately equal to the skin depth. The skin effect shrinks the effective cross-section of the conductor increasing the resistance proportionally to $\sqrt{f}$. Therefore, the conductor loss depends on the material properties, geometry of the conductor and is frequency-dependent.

At the same time the resistivity of metals is temperature-dependent. If the temperature T changes within several hundred of K the temperature dependence of electrical resistance is can be approximated by a linear function [7].

$$\rho(T) \approx \rho_0[1 + \alpha_T(T - T_0)], \quad (5)$$

where ρ_0 is the resistivity (in Ω·m) at the reference temperature T_0, and α_T is the temperature coefficient of resistivity, (in $°C^{-1}$, or K^{-1}).

Due to high current consumption the operating temperature of modern equipment is typically considerably higher than room temperature [8]. The temperature is high enough to noticeably increase of resistivity and, therefore the attenuation of the transmission line. The example of the increased loss due to temperature is shown on Figure 1.1 Simulations were done for a 5000 mil long stripline structure having 3 mil trace width and 9.1 mil thickness of the bulk dielectric. Dielectric has the dielectric constant (DK) of 4 and dissipation factor (DF) equal to 0.008 (medium-loss dielectric). Applying Eq.4 and using $\rho_0 = 1.724 \cdot 10^{-8}\ \Omega\mathrm{m}$ (nominal value for pure copper), $\alpha_T = 0.00393\ 1/°\mathrm{C}$, $T_0 = 25\ °\mathrm{C}$ the resistivity at $T = 25\ °\mathrm{C}$ and $T = 125\ °\mathrm{C}$ is calculated. After that the transmission coefficient of the line is calculated using the model in Advanced Design System [45]. The resulting coefficients are shown in Figure 1.1. As

can be seen, increasing the temperature by 100 °C leads to 1 dB difference at 50 GHz and cannot be neglected in some cases.

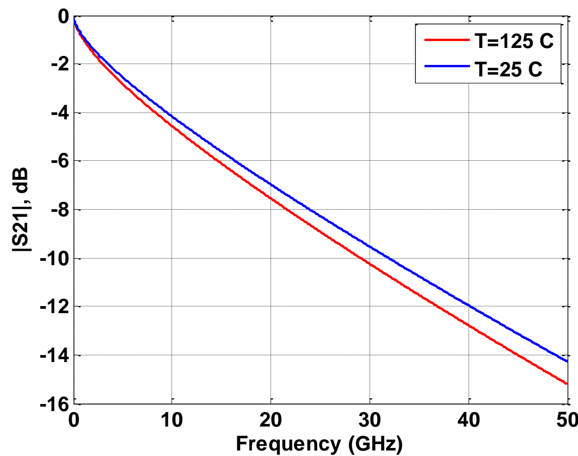

Figure1.1. Modeled transmission coefficients of stripline at 25 ℃ and 125 ℃

The purpose of Chapter 2 of the thesis is to study the temperature dependency of resistance for different copper types used in PCB design.

As was said above the conductor surface roughness is an important factor affecting the performance of high-speed transmission lines. Real PCB traces are not smooth and the surface quality depends on technological process used during the PCB fabrication [9]. Also copper traces in transmission lines are intentionally made rough to promote adhesion to the dielectric. Typically "root-mean-squared" (RMS) value of roughness is calculated as [10]

$$h_{rms} = \sqrt{\mathrm{E}\left[\left(X - x_{\mu}\right)^{2}\right]}, \tag{6}$$

where X is the profile function, x_{μ} is the mean value of X and E denotes as expected value operator.

There are other parameters of surface roughness that can be found in literature. For example R_z, referred to as ten point height, is the average absolute value of the five highest peaks and the five lowest valleys. The h_{rms} (or R_q in literature) typically is 0.25-0.7μm for hyper very low profile (HVLP) foils, 0.3-1.0μm for very low profile (VLP)

foils, and 1.0-2.0μm for standard profile (STD) foils [1, 9, 10, 48]. The examples of several foil type profiles are presented in Figure 1.2.

Figure 1.2. Optical microscopic images of roughness. From left to right: STD (standard), VLP (very low profile), HVLP (hyper very low profile)

At frequencies starting from approximately 2GHz the skin depth becomes comparable to the RMS height of the surface roughness, impacting the flow of the current considerably.

Modern commercial software tools have models for conductor surface roughness in transmission lines, however all of them provide insufficient accuracy (in-depth review of models is presented in Section 3). Examples are presented in Figure 1.3.

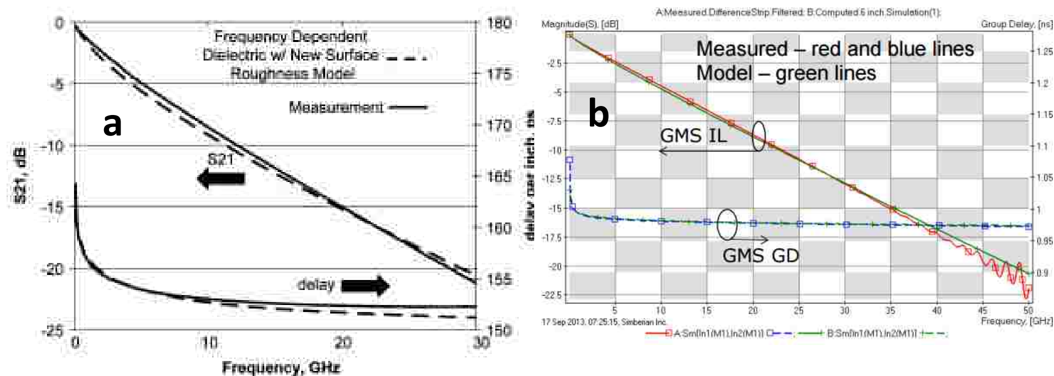

Figure1.3. Hall Hemispherical model used in ADS [5] (a), GMS model developed in Simberian Inc. [11] (b)

In order to improve our understanding of the physical processes in striplines with rough conductors a full-wave model is proposed in Section 3. It might be used in the future as the basis of a truly physics-based roughness model.

2. MEASUREMENT OF COPPER RESISTIVITY

Pure copper has relatively low electrical resistivity among commercially useful metals. On the other hand the resistivity of different copper types used for PCB fabrication might vary [12].What is worse is that thermal processing of copper (like annealing) affects the resistivity profoundly [13]. Because of this it becomes impossible in many cases to predict the actual resistivity of conductors in PCBs.

Resistivity is temperature dependent, if the temperature increases, resistivity increases as well. This chapter will outline the methodology for temperature dependence measurements of the resistivity. A quick explanation of four probe technique is provided. Then, the methodology is applied to the eleven copper types used in PCB design. The resistivity and conductivity values as well as temperature coefficients are calculated and discussed.

2.1. BACKGROUND

Electrical resistivity of copper and its temperature dependence has been investigated and reported by many groups over more than a century. The earliest report is published by Lorenz [14] in 1881. In his work he obtained the resistivity values of $2.18 \cdot 10^{-8}$ Ω·m and $2.95 \cdot 10^{-8}$ Ω·m at 273K and 373K correspondingly. Next, the report of Jaeger and Diesselhorst [15] was published in 1900 where they performed measurements at 291K and 373K and the reported resistivity is $1.81 \cdot 10^{-8}$ Ω·m and $2.40 \cdot 10^{-8}$ Ω·m. Referring to J.H. Dellinger [16] work published in 1900 the reported temperature coefficient is 0.00394 but resistivity value is not provided. In work of Niccolai [17] made at 1908 the measurements were done from 84K to 673K with reported changes in resistivity from $0.302 \cdot 10^{-8}$ Ω·m to $4.093 \cdot 10^{-8}$ Ω·m. The 1914 report of Northrup [18] presents the data starting from room temperature to well above the melting point. In 1914 Stratton [19] published work with obtained resistivity value and temperature coefficient. Then, in 1927 Gruneisen and Goens [20] did measurements on numerous copper specimens from 21.2K to 273K. In [21] Laubitz did the measurements of the annealed 99.999% pure copper from 273K to1272K. Moore et al. measured the same samples Laubitz used but temperature was varied from 85K to 375K. There are numerous works by other authors dedicated to investigation of copper

resistivity under temperature influence. Explicit data analysis was performed by Matula in 1979 [7]. In his work he consolidated all reported data related to resistivity of copper and provided the recommended values at different temperatures which partly are given in Table 2.1.

Table 2.1. Values for the electrical resistivity and temperature coefficients of annealed copper

Author	Temperature, K/℃	Resistivity , Ω·m	Temp. Coefficient, 1/℃
Matula	300/27	$1.725 \cdot 10^{-8}$	N/A
	350/77	$2.063 \cdot 10^{-8}$	
Dellinger	293/20	N/A	0.00394
Stratton	293/20	$1.724 \cdot 10^{-8}$	0.00393

The conductivity of a material is defined by differential form of Ohm's law as

$$J = \sigma E, \tag{7}$$

where J is the current density and E is the electric field in the direction of current flow. It is useful to express conductivity in terms of more familiar voltage and current. The current density is given by

$$J = I/A, \tag{8}$$

where I is the current in Amperes and A is the cross sectional area of the conductor. The electric field is given:

$$E = V/L, \tag{9}$$

where V is the total voltage drop along the conductor sample and L is the length of the sample. Rearranging (7) and substituting to (8) and (9) gives:

$$\rho = \frac{1}{\sigma} = \frac{E}{J} = \frac{A \cdot V}{L \cdot I} = \frac{R \cdot A}{L} \quad (10)$$

where ρ is the sample resistivity (in $\Omega \cdot$m) and R is the sample's measurable resistance (in Ω). Thus by measuring the resistance directly (or the voltage and current), and knowing the sample's physical dimensions, the resistivity or its conductivity can be calculated.

2.1.1. Four-Probe Technique. For the resistance measurements of the conductors the four probe technique is typically used [22],[23]. The schematic of the four probe technique is shown in Figure 2.1. It consists of the current source, ampere-meter, and voltmeter. Connection of the current source and voltmeter to the sample is performed using the probes. Then, current I is made to flow between the probes as shown by red arrows in Figure 2.1. Voltage V is measured between the two probes, ideally without drawing any current and avoiding the resistance error factor (including contact resistance). From the ratio of measured voltage and current the resistance can be determined using the Ohm law.

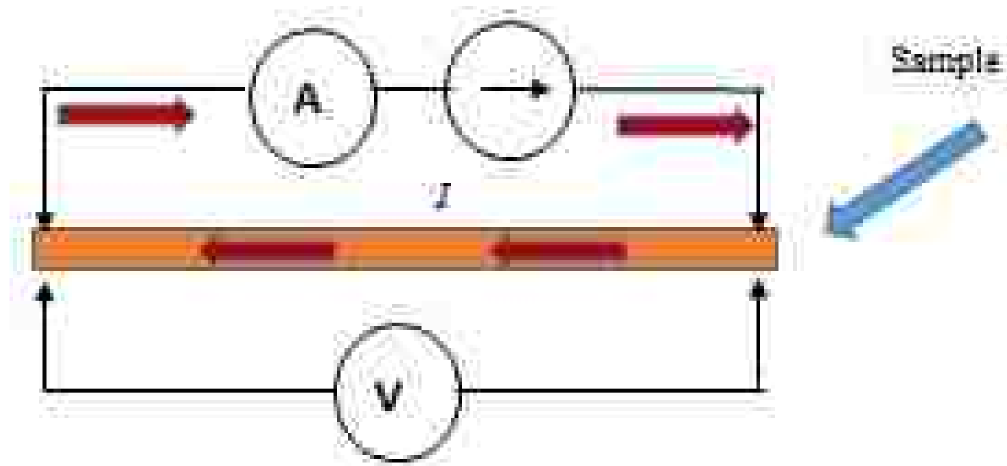

Figure 2.1. Schematic of Four - Point Probe Technique

2.1.2. Setup. For the Resistance measurements the LCR meter HP4263b with custom probes is used. Probes are made using pogo pins and coax cables and are shown in Figure 2.2. The LCR meter is the instrument which is usually used for inductance (L), capacitance (C) and resistance (R) measurements. It has four terminals, two can measure voltage across the sample and another two apply current to the sample according to the diagram in Figure. 2.1. Although the measurements are performed at 100 Hz, the skin effect at this frequency is negligible and the results are indistinguishable from the measurements at DC

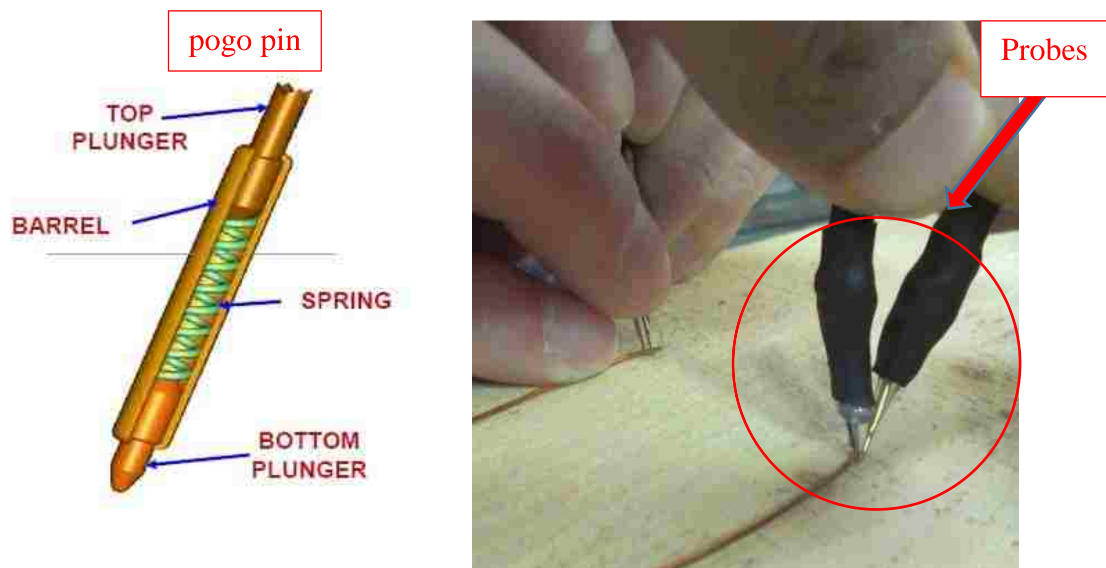

Figure 2.2. Pogo pin (left), Customized probes for resistivity measurements (right)

For the temperature dependence measurements the device under test (DUT) must be heated up for as long as the measurement requires. To heat up the DUT the hot plate with the adjustable temperature is used. The temperature range of interest is from room temperature 25°C (298 K) to 100°C (373K).Two thermocouples are connected to the DUT to monitor the temperature and two precision digital thermometers (ΔT=0.1 K) are used to read the temperature from thermocouples. The schematic of the setup is shown in Figure 2.3.

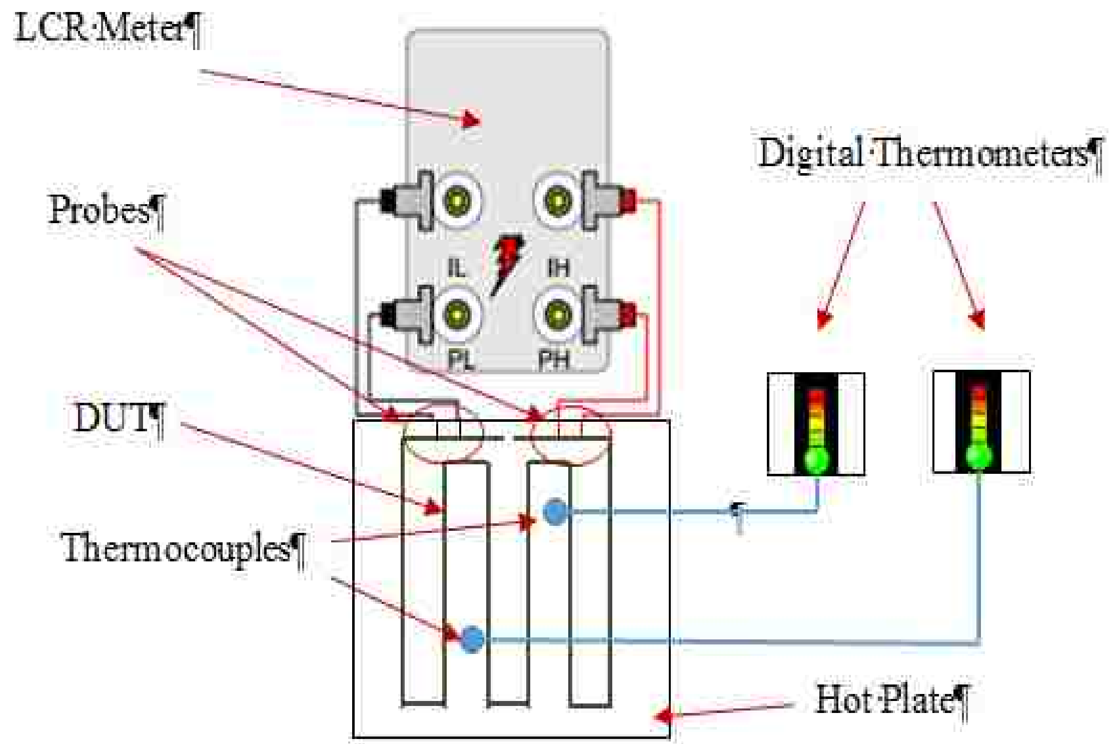

Figure 2.3. Setup schematic for resistance measurements

The main problem is to maintain the homogeneous temperature distribution over the hot plate. Requirement for this study is that the discrepancy of temperature should not exceed 1°C. In order to meet it, the DUT is put between two metal plates. The bottom plate has around 10 mm thickness and the top plate is 2 mm thick and has thermal Mylar tape on it to avoid shorting the sample. The bottom plate is then heated by the hot plate and the top one helps to keep the DUT temperature steady. The setup implementation is presented in Figure 2.4. The “sandwich” structure provides the homogenous temperature distribution over the entire DUT needed for this study. To be able to land the probes and perform the measurement the 1.5x1.5 cm window is cut in the top plate. Provided space is enough to land four probes connected to the LCR Meter. Window of this size does not affect the accuracy of the measurement because the rest of the DUT stays covered and the bottom plate has not been changed.

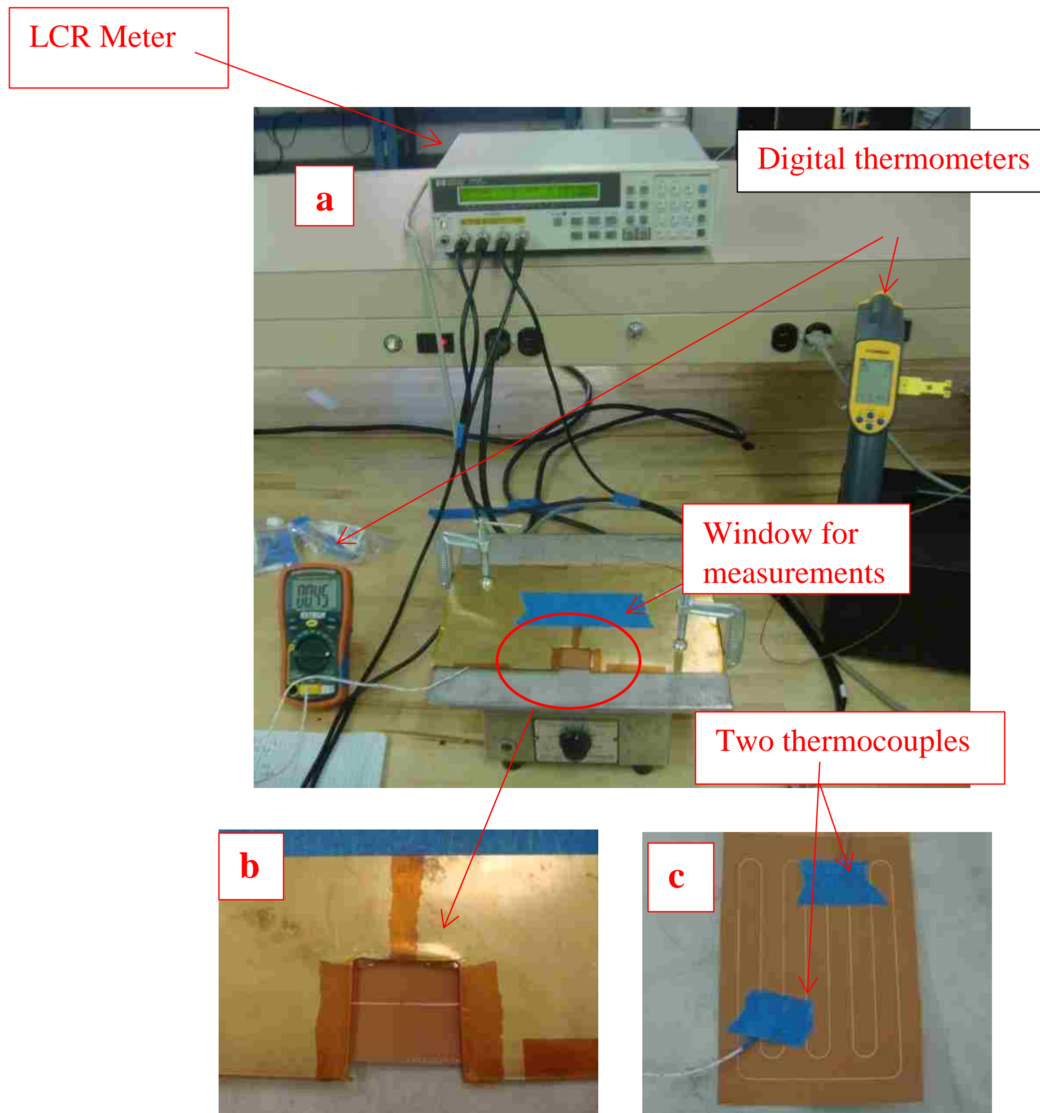

Figure 2.4. Setup for resistance measurements (a), window for probes landing (b), two thermocouples placed on the DUT (c)

To summarize the procedure for temperature dependency investigation, the following steps should be taken:

- Put the DUT between two plates and start heating
- Monitor the temperature until it reaches the desired one
- Take Resistance measurements applying four probes of the LCR Meter

2.1.3. DUT Description. For the temperature dependency investigation the set of copper coupons has been fabricated. The top layer of coupon is presented in Figure 2.5. The bottom layer of all coupons is solid copper. Totally eleven copper types have been provided for this study. Every copper type contains 30 coupons and every ten of them have different trace width. The specific copper types will be listed latter.

The length of each sample is 1 m. As it is shown in Figure 2.5 each sample has special form to minimize the occupied space and to put the sample ends close to each other.

The main feature of these coupons is a 0.5 mm gap to be able to place probes for measurements.

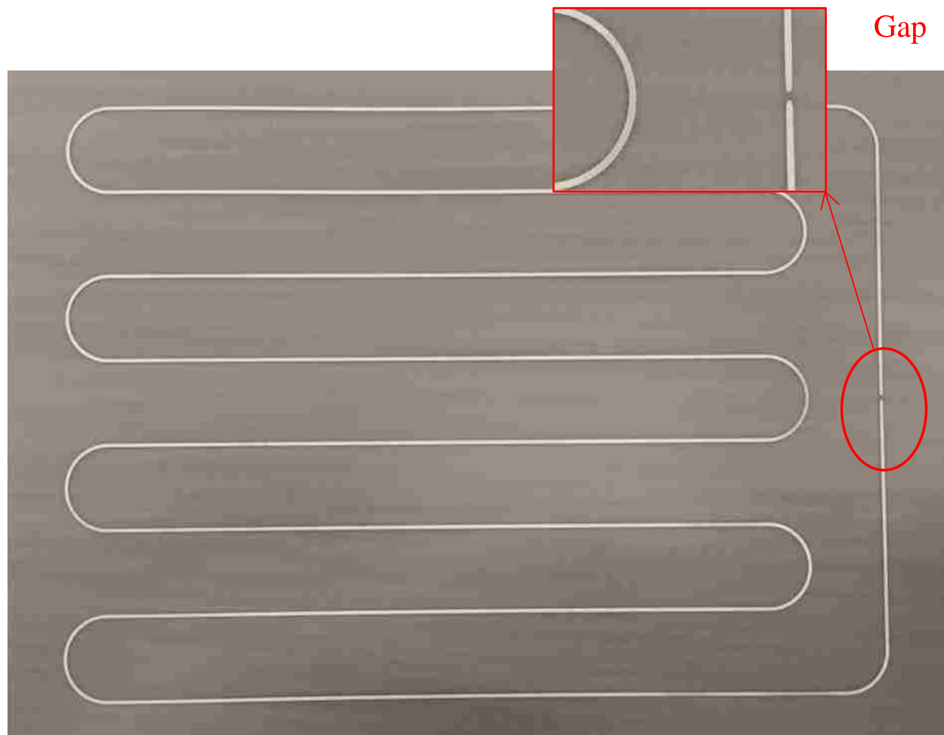

Figure 2.5. Top layer of tested coupon

Another parameter needed for resistivity calculation is a cross sectional area. The cross section is taken by cutting the sample by the plane normal to the current flow. For accurate calculation several traces were cut, polished and measured using an optical microscope. One of the cross sections with measured thickness is presented in Figure 2.6.

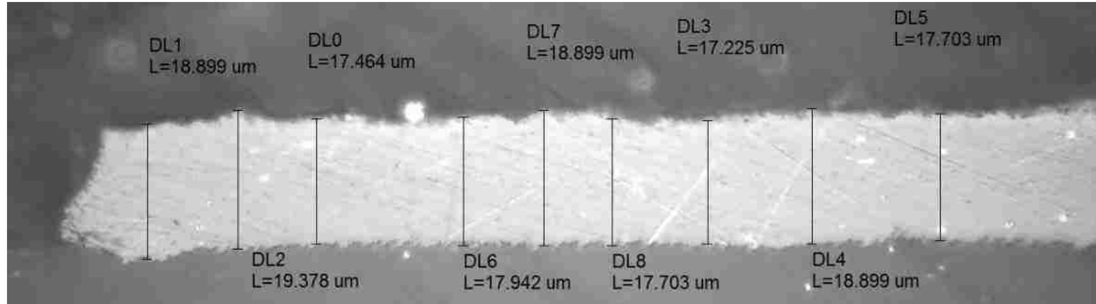

Figure 2.6. The cross section of the tested trace

2.1.4. Uncertainty Estimation. The usual way to quantify the spread of measured data is standard deviation. The standard deviation of a set of numbers tells how different the individual readings typically are from the average of the set. The bias-corrected standard deviation for a series of n measurements can be expressed mathematically as:

$$S = \sqrt{\frac{\sum_{i=1}^{n}(x_i - \bar{x})^2}{n-1}}, \tag{11}$$

where $\bar{x}$ is the arithmetic mean of measured data. When a set of several repeated readings has been taken the uncertainties should be properly estimated. All contributing uncertainties should be expressed at the same confidence level, by converting them into standard uncertainties. Standard uncertainty Δu (or Standard Error (SE)) is determined as the standard deviation of the mean [24] and calculated as [24-28]:

$$\Delta u = \frac{S}{\sqrt{n}} \tag{12}$$

This expression reflects the fact that standard uncertainty decreases with increasing the number of measurements.

Oftentimes, the uncertainty should be calculated for quantity f which depends on several variables x_i with their own uncertainties. In this case the uncertainty in f is determined as [24-28]:

$$\Delta u_f = \sqrt{\sum_{i=1}^{N} \left(\frac{\partial f(x_i)}{\partial x_i} \Delta u(x_i)\right)^2}. \tag{13}$$

Consider the Cross sectional area of the trace given by

$$A = W \cdot T, \tag{14}$$

where W is the trace width and T is its thickness. Then applying (13) the uncertainty in the area is given by

$$\Delta A = (W \cdot T)\sqrt{\left(\frac{\Delta W}{W}\right)^2 + \left(\frac{\Delta T}{T}\right)^2}, \tag{15}$$

where the width uncertainty ΔW and thickness uncertainty ΔT are calculated using (11). W and T are the mean values calculated from microscopic photos. The calculated area and its uncertainties are consolidated in Table 2.2.

Table 2.2. Thickness, width and area of traces

Thickness, μm	18.02±0.15		
Width, μm	488.24±0.59	493.62±1.20	499.00±0.60
Area, μm^2	8798.08±73.99	8877.01±76.77	8991.98±75.41

Considering the relative uncertainties of width $\frac{\Delta W}{W} = \frac{0.59}{488.24} = 1.2 * 10^{-3} = 0.12\%$, thickness $\frac{\Delta T}{T} = \frac{0.67}{18.02} = 8.3 * 10^{-3} = 0.83\%$. and calculated area $\frac{\Delta A}{A} = \frac{73.99}{8798.08} =$

0.84%, it is obvious that the thickness has the dominating contribution to the total uncertainty.

The uncertainty in resistivity can be derived by substituting (10) to (13):

$$\Delta\rho = \sqrt{\left(\frac{A}{L}\cdot\Delta R\right)^2 + \left(\frac{R}{L}\cdot\Delta A\right)^2 + \left(-\frac{RA}{L^2}\cdot\Delta L\right)^2} \quad (16)$$

Equation (16) shows that the total uncertainty of resistivity depends on the corresponding uncertainties of area, sample length and measured resistance. The uncertainty related to sample length is not considered and neglected. The uncertainty in resistance depends on particular setup and measurement method and was 0.1% according to the LCR meter specification. There are several other type of errors such as systematic ones. Only random errors are considered in this work.

2.1.5. Results and Discussion. Measurements of resistance were done using LCR meter HP4263b for 330 samples (11 foil types by 30 samples) at room temperature (25 °C), 50 °C and 100 ˚C. Applying (10) the resistivity and conductivity values have been calculated and presented in Tables 2.4-2.5. Results were confirmed by measurements in the Material Research Center (MRC) at room temperature using another, much more expensive facility (Allesi C4S), based on the same 4-point technique. Picture of Allesi C4S instrument is presented in Figure 2.7. Discrepancy in resistivity obtained by two independent measurements (LCR meter at AC and Allesi C4S at DC) does not exceed 0.5% and is presented in Table 2.3. The measurements at 50 °C and 100 °C have not been verified due to Allesi C4S limitations. Nevertheless, such low difference in results indicates that the instrument error has low contribution into total uncertainty of calculated resistivity value.

The results show that the conductivity values at room temperature of different copper types are 12.5% lower on average than the nominal pure copper value $\sigma = 5.80 \cdot 10^7$ S/m. For convenience the obtained results are presented also in Figure 2.8 and Figure 2.9.

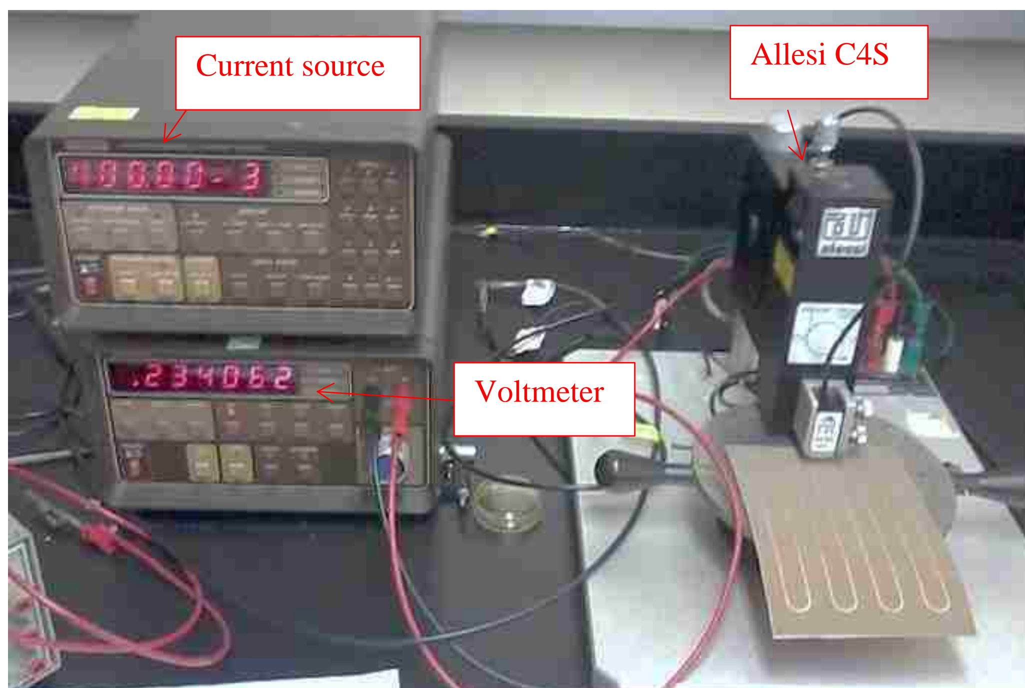

Figure 2.7 Allesi C4S 4-point probe

Table 2.3. Comparison of conductivity obtained by two methods
(3 copper types are shown)

type/setup	Allesi, Conductivity S/m	LCR Meter, Conductivity S/m
OM ML	$4.876 \cdot 10^7 \pm 0.044 \cdot 10^7$	$4.873 \cdot 10^7 \pm 0.042 \cdot 10^7$
OM MLS	$5.141 \cdot 10^7 \pm 0.046 \cdot 10^7$	$5.153 \cdot 10^7 \pm 0.045 \cdot 10^7$
NY NPV	$4.955 \cdot 10^7 \pm 0.057 \cdot 10^7$	$4.931 \cdot 10^7 \pm 0.051 \cdot 10^7$

Table 2.4. Conductivity at room temperature, 50 °C and 100 °C

type	$\sigma, S/m$ at Room Temperature	$\sigma, S/m$ At 50 °C	$\sigma, S/m$ At 100 °C
OM ML	$4.873 \cdot 10^7 \pm 0.042 \cdot 10^7$	$4.441 \cdot 10^7 \pm 0.038 \cdot 10^7$	$3.730 \cdot 10^7 \pm 0.033 \cdot 10^7$
OM MLS	$5.153 \cdot 10^7 \pm 0.045 \cdot 10^7$	$4.687 \cdot 10^7 \pm 0.041 \cdot 10^7$	$3.963 \cdot 10^7 \pm 0.037 \cdot 10^7$
OM VSP	$4.984 \cdot 10^7 \pm 0.042 \cdot 10^7$	$4.513 \cdot 10^7 \pm 0.039 \cdot 10^7$	$3.804 \cdot 10^7 \pm 0.032 \cdot 10^7$
NY NPHD	$5.073 \cdot 10^7 \pm 0.044 \cdot 10^7$	$4.586 \cdot 10^7 \pm 0.039 \cdot 10^7$	$3.874 \cdot 10^7 \pm 0.034 \cdot 10^7$
NY NPV	$4.931 \cdot 10^7 \pm 0.051 \cdot 10^7$	$4.471 \cdot 10^7 \pm 0.045 \cdot 10^7$	$3.777 \cdot 10^7 \pm 0.037 \cdot 10^7$
CF TW-B	$5.152 \cdot 10^7 \pm 0.044 \cdot 10^7$	$4.696 \cdot 10^7 \pm 0.041 \cdot 10^7$	$3.947 \cdot 10^7 \pm 0.035 \cdot 10^7$
OM VLP	$4.809 \cdot 10^7 \pm 0.041 \cdot 10^7$	$4.368 \cdot 10^7 \pm 0.038 \cdot 10^7$	$3.694 \cdot 10^7 \pm 0.032 \cdot 10^7$
CF BF-TZA	$4.780 \cdot 10^7 \pm 0.042 \cdot 10^7$	$4.350 \cdot 10^7 \pm 0.039 \cdot 10^7$	$3.687 \cdot 10^7 \pm 0.035 \cdot 10^7$
FUR FV-WS	$4.840 \cdot 10^7 \pm 0.042 \cdot 10^7$	$4.398 \cdot 10^7 \pm 0.038 \cdot 10^7$	$3.722 \cdot 10^7 \pm 0.032 \cdot 10^7$
GD RTC	$5.130 \cdot 10^7 \pm 0.044 \cdot 10^7$	$4.662 \cdot 10^7 \pm 0.041 \cdot 10^7$	$3.916 \cdot 10^7 \pm 0.038 \cdot 10^7$
CF TW	$5.111 \cdot 10^7 \pm 0.046 \cdot 10^7$	$4.644 \cdot 10^7 \pm 0.042 \cdot 10^7$	$3.913 \cdot 10^7 \pm 0.035 \cdot 10^7$

Table 2.5. Resistivity at room temperature, 50 °C and 100 °C

type	$\rho, \Omega \cdot m$ at Room Temperature	$\rho, \Omega \cdot m$ At 50 C	$\rho, \Omega \cdot m$ At 100 C
OM ML	$2.053 \cdot 10^{-8} \pm 0.017 \cdot 10^{-8}$	$2.252 \cdot 10^{-8} \pm 0.019 \cdot 10^{-8}$	$2.681 \cdot 10^{-8} \pm 0.024 \cdot 10^{-8}$
OM MLS	$1.944 \cdot 10^{-8} \pm 0.017 \cdot 10^{-8}$	$2.134 \cdot 10^{-8} \pm 0.019 \cdot 10^{-8}$	$2.524 \cdot 10^{-8} \pm 0.024 \cdot 10^{-8}$
OM VSP	$2.007 \cdot 10^{-8} \pm 0.017 \cdot 10^{-8}$	$2.216 \cdot 10^{-8} \pm 0.019 \cdot 10^{-8}$	$2.629 \cdot 10^{-8} \pm 0.022 \cdot 10^{-8}$
NY NPHD	$1.972 \cdot 10^{-8} \pm 0.017 \cdot 10^{-8}$	$2.181 \cdot 10^{-8} \pm 0.019 \cdot 10^{-8}$	$2.581 \cdot 10^{-8} \pm 0.023 \cdot 10^{-8}$
NY NPV	$2.029 \cdot 10^{-8} \pm 0.021 \cdot 10^{-8}$	$2.237 \cdot 10^{-8} \pm 0.022 \cdot 10^{-8}$	$2.647 \cdot 10^{-8} \pm 0.026 \cdot 10^{-8}$
CF TW-B	$1.943 \cdot 10^{-8} \pm 0.017 \cdot 10^{-8}$	$2.129 \cdot 10^{-8} \pm 0.019 \cdot 10^{-8}$	$2.534 \cdot 10^{-8} \pm 0.022 \cdot 10^{-8}$
OM VLP	$2.081 \cdot 10^{-8} \pm 0.018 \cdot 10^{-8}$	$2.289 \cdot 10^{-8} \pm 0.020 \cdot 10^{-8}$	$2.707 \cdot 10^{-8} \pm 0.024 \cdot 10^{-8}$
CF BF-TZA	$2.094 \cdot 10^{-8} \pm 0.018 \cdot 10^{-8}$	$2.299 \cdot 10^{-8} \pm 0.021 \cdot 10^{-8}$	$2.712 \cdot 10^{-8} \pm 0.026 \cdot 10^{-8}$
FUR FV-WS	$2.064 \cdot 10^{-8} \pm 0.018 \cdot 10^{-8}$	$2.274 \cdot 10^{-8} \pm 0.020 \cdot 10^{-8}$	$2.687 \cdot 10^{-8} \pm 0.027 \cdot 10^{-8}$
GD RTC	$1.963 \cdot 10^{-8} \pm 0.017 \cdot 10^{-8}$	$2.145 \cdot 10^{-8} \pm 0.019 \cdot 10^{-8}$	$2.553 \cdot 10^{-8} \pm 0.026 \cdot 10^{-8}$
CF TW	$1.958 \cdot 10^{-8} \pm 0.018 \cdot 10^{-8}$	$2.153 \cdot 10^{-8} \pm 0.019 \cdot 10^{-8}$	$2.556 \cdot 10^{-8} \pm 0.023 \cdot 10^{-8}$

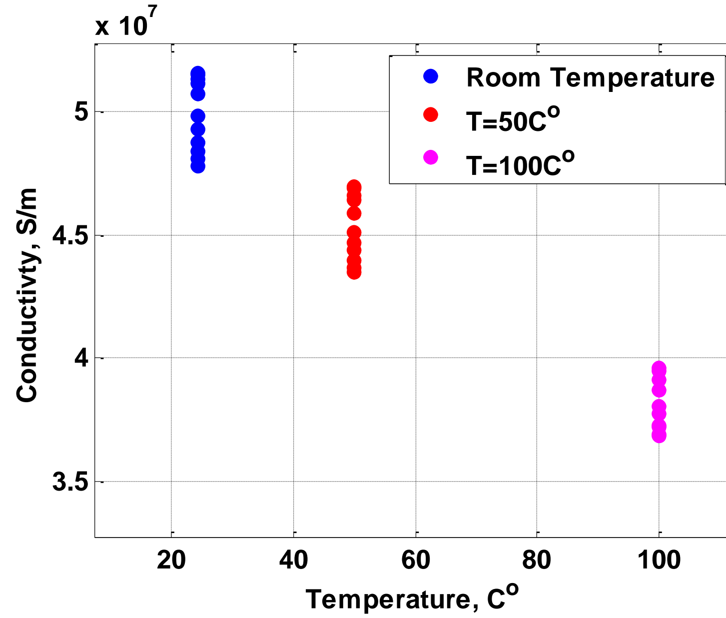

Figure 2.8. Conductivity over temperature for all tested copper types

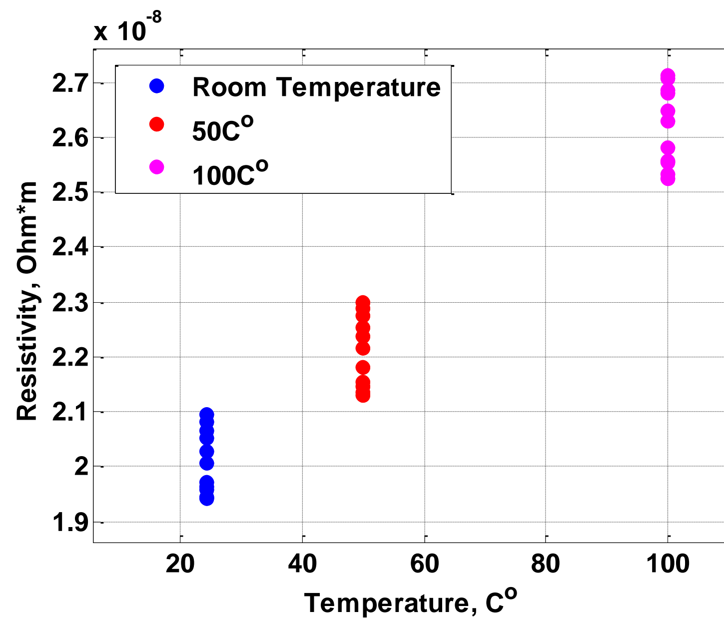

Figure 2.9. Resistivity over temperature for all tested copper types

The temperature coefficients were calculated by inverting the equation (5) and fitting resistivity values between 25 °C and 100 °C by a linear function. The calculated (fitted) resistivity temperature dependency is plotted in Figure 2.10 along with the measured one.

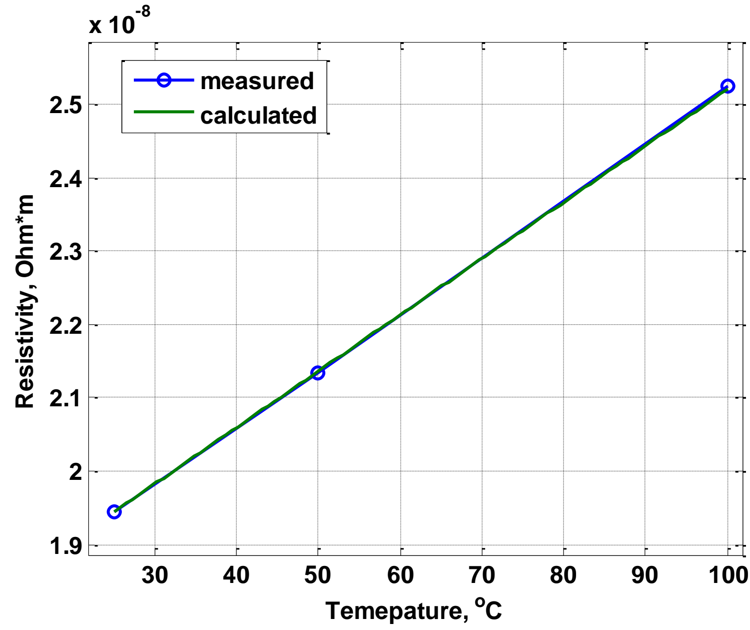

Figure 2.10. Resistivity vs. temperature

Performing the calculation for every measured copper type, the temperature coefficients have been extracted and presented in Table 2.6.

Table 2.6. Temperature coefficients for tested copper foils

foil type	temperature coefficient, $1/°C$	Foil type	temperature coefficient, $1/°C$
OM ML	$4.07 \cdot 10^{-3}$	OM VLP	$4.00 \cdot 10^{-3}$
OM MLS	$3.97 \cdot 10^{-3}$	CF BF-TZA	$3.95 \cdot 10^{-3}$
OM VSP	$4.13 \cdot 10^{-3}$	FUR FV-WS	$4.02 \cdot 10^{-3}$
NY NPHD	$4.12 \cdot 10^{-3}$	GD RTC	$4.00 \cdot 10^{-3}$
NY NPV	$4.10 \cdot 10^{-3}$	CF TW	$4.06 \cdot 10^{-3}$
CF TW-B	$4.05 \cdot 10^{-3}$		

2.2. SUMMARY

The LCR Meter with custom probes can be used for the efficient and accurate measurements of copper resistivity. Resistivity values calculated based on LCR meter measurements converge to those calculated based on measurements taken at the Material Research Center using Allesi C4S at room temperature. Calculated conductivity values at room temperature of different copper types are 12.5% lower on average than the nominal pure copper value $\sigma = 5.80 \cdot 10^7$ S/m.

Further application of Allesi C4S for the temperature dependency measurements is not possible due to its configuration. For this purpose the LCR meter was successfully utilized at 50 °C and 100°C providing expected linear behavior for resistivity. Setup for these measurements is easy to implement and does not requires using the environmental chamber, achieving the temperature discrepancy below 1 °C. Resistivity values of tested copper types show approximately linear behavior in 25-100 ℃ temperature range. Overall, the conductivity/resistivity values change with temperature and average difference between room temperature and 100C is 30%. Calculated temperature coefficients have good agreements with results presented in [8]. Particularly, the reported temperature coefficients are in the range form $3.69 \cdot 10^{-3}$ 1/℃ to $4.09 \cdot 10^{-3}$ 1/℃ at 20C and the measured results are in the range from $3.95 \cdot 10^{-3}$ 1/℃ to $4.13 \cdot 10^{-3}$ 1/℃. Also performed uncertainty estimation shows that the main contribution into the total error is due to the uncertainty in the trace thickness. In order to reduce the error, the actual area of tested samples has to be extracted from the microscopic images of the trace cross section.

3. SURFACE ROUGHNESS MODELING

In real PCBs the traces are never smooth and have rough surface causing the additional loss [29-31]. Moreover, loss related to surface roughness increases with frequency and affects the SI performance. Since the clock frequencies of modern high speed devices are in the multi-GHz region the effect of surface roughness cannot be neglected in general.

3.1. EXPERIMENTAL INVESTIGATION OF SURFACE ROUGHNESS EFFECTS

For the experimental investigation of the influence of the surface roughness on losses the set of PCB has been manufactured with different widths and foil types. Totally 12 PCB sets were fabricated with every set consisting of six identical PCBs. All test lines are 50 Ohm single ended (SE) striplines and the Megtron6 is used as laminate dielectric. The picture of a typical test vehicle is given in Figure 3.1. The test board has a “through-reflect-line” (TRL) calibration pattern. the valid frequency range of the calibration pattern is at least up to 30 GHz.

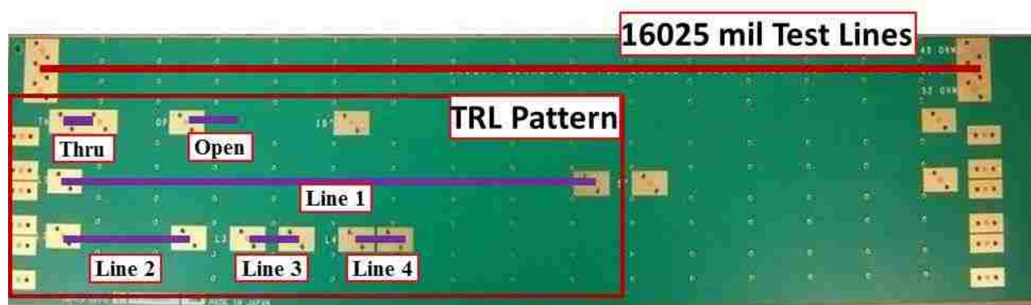

Figure 3.1. Picture of the test vehicle

The launch structure is a surface pad designed to accept a flange-mount, compression-fit SMA connectors. The 3.5 mm SMA connectors are mounted on top of the PCB and are used for excitation. The drawing of the SMA connector is presented on Figure 3.2

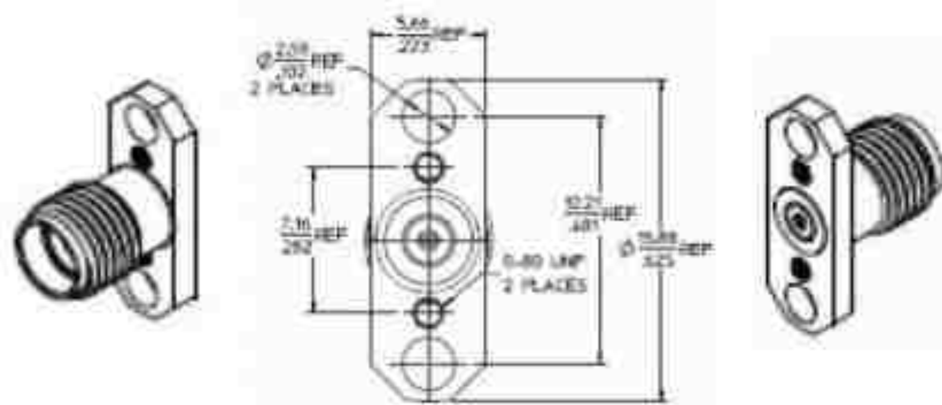

Figure 3.2. Drawing of SMA connector

Three foil types have been implemented for this research: Standard foil (STD), very low profile (VLP), and hyper low profile (HVLP). Roughness parameters for each of them are provided in Table 3.1.

Table 3.1. Roughness parameters for three tested foil types [47]

Resist Side	h_{rms}, µm	Peak to Peak, µm
STD	1.0-2.0	7.0-12.0
VLP	0.3-0.4	3.0-4.0
HVLP	0.25-0.35	2.0-3.0
After alt. Oxide	h_{rms}, µm	Peak to Peak, µm
STD	1.0-2.0	7.0-12.0
VLP	0.6-1.0	6.0-8.0
HVLP	0.5-0.7	4.0-6.0

3.1.1. Measurement Results and Observations. After the TRL calibration the S-parameters of the 16 inch test lines on all PCBs have been measured. Measured insertion loss of 12 PCBs with different roughness and trace width are illustrated by Figure 3.3.

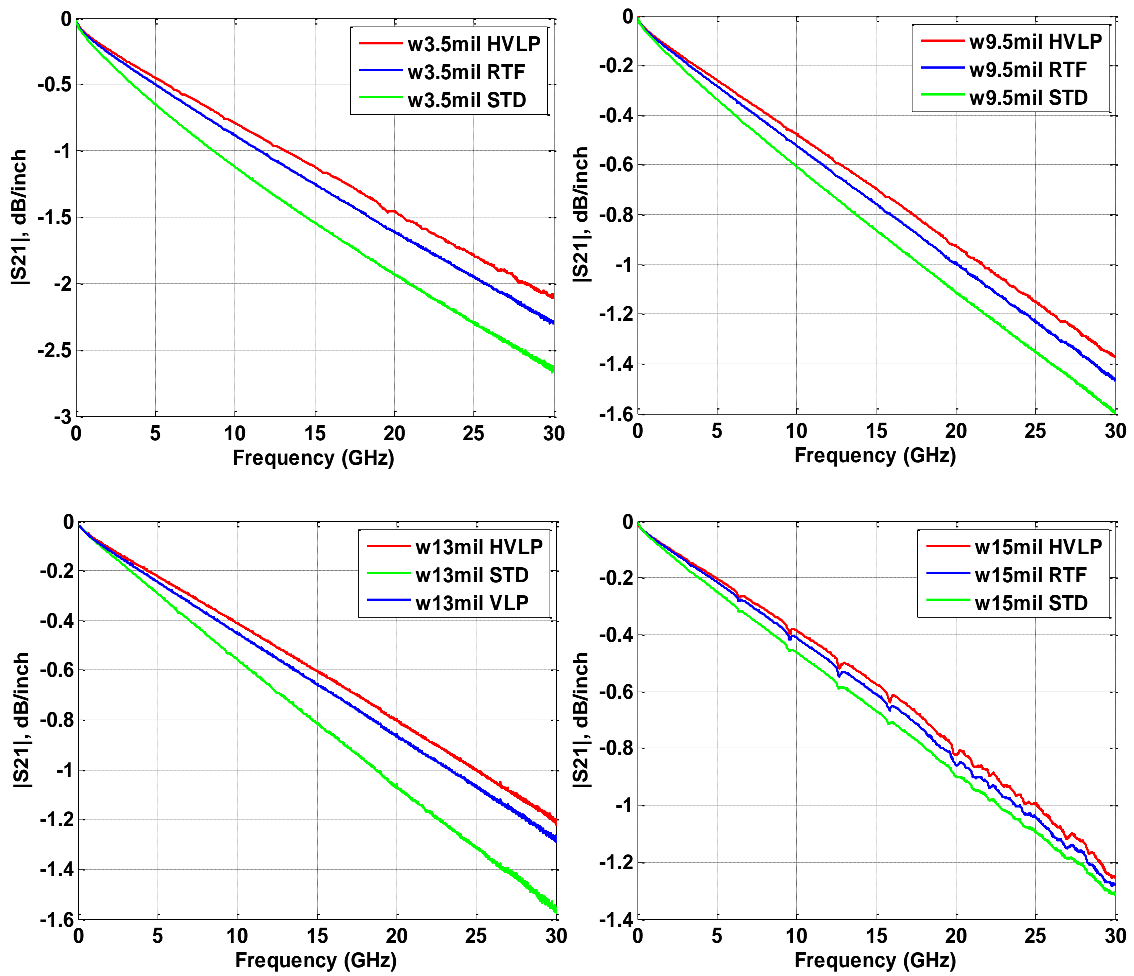

Figure 3.3. $|S_{21}|$ per inch for the entire PCBs set

The obtained results show that, first of all, the insertion loss increases with the magnitude of roughness as expected, also the additional loss due to the roughness increases with frequency. At the same time the impact of the surface roughness on the total loss decreases for wider traces. The difference in losses with respect to HVLP at 15GHz are given in Table 3.2 illustrating these effects.

Table 3.2. Difference in loss for different trace width at 15GHz

	3.5mil	9.5mil	13mil	15mil
STD-HVLP,%	37.8	23.9	37.7	16.8
VLP-HVLP,%	11.8	8.8	8.6	6.4

Another unexpected observation is that the slope of S_{21} curve increases with frequency, which is particularly visible for HVLP traces.

Attenuation coefficient due to the dielectric loss is proportional to the frequency as $\alpha_d = C \cdot \omega \cdot \tan\delta$ where C is the per unit length (pul) capacitance of the line [6]. Since the conductor loss increases proportionally to the $\sqrt{\omega}$ (see [1]) at sufficiently high frequencies the dielectric loss dominates and one should expect almost linear increase of loss factor for non-dispersive dielectrics. The measurements in Figure 3.3 however show noticeably non-linear behavior at high frequencies. This behavior was observed in other research groups independently, for example, as it is shown in Figure 3.4.

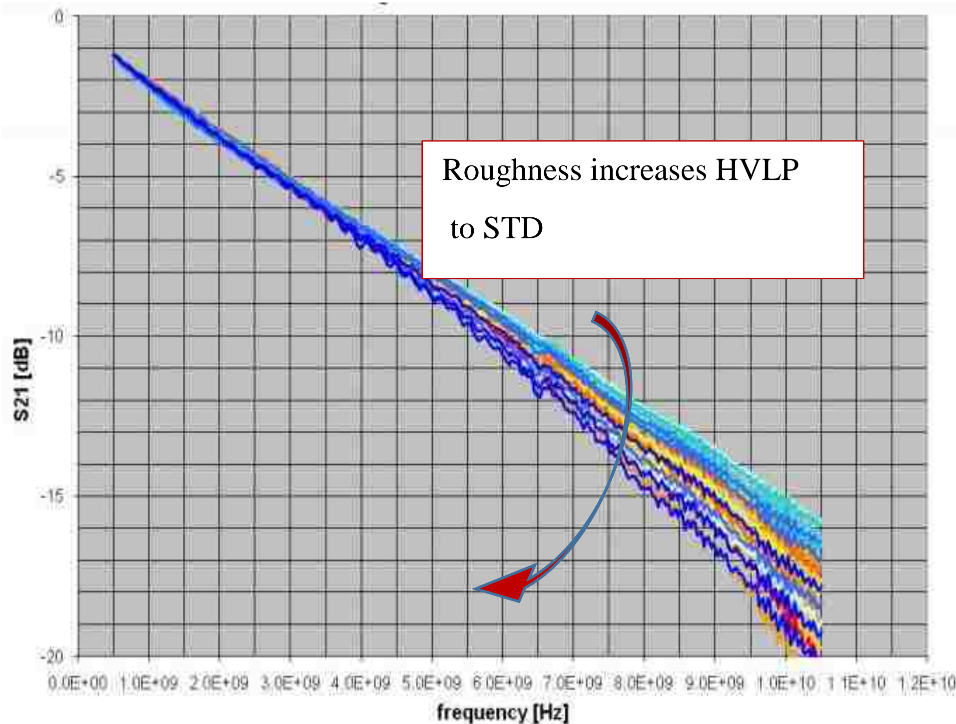

Figure 3.4. Nonlinear behavior of the insertion loss due to the surface roughness [29]

In principle the increase of the slope of S_{21} could be explained by the frequency-dependent loss in the dielectric in the multi-GHz frequency range (as is done in [32]), however on the other hand, there are reports indicating that the low-loss dielectrics typically used in the PCB design are very low-dispersive above 5 GHz and have nearly frequency independent tanδ (examples are presented in Figure 3.5 (resonator method) and

Figure 3.6 (transmission line method)) [33,48]. If it is true, the non-linearity of the attenuation constant must be attributed solely to the effects of conductor surface roughness.

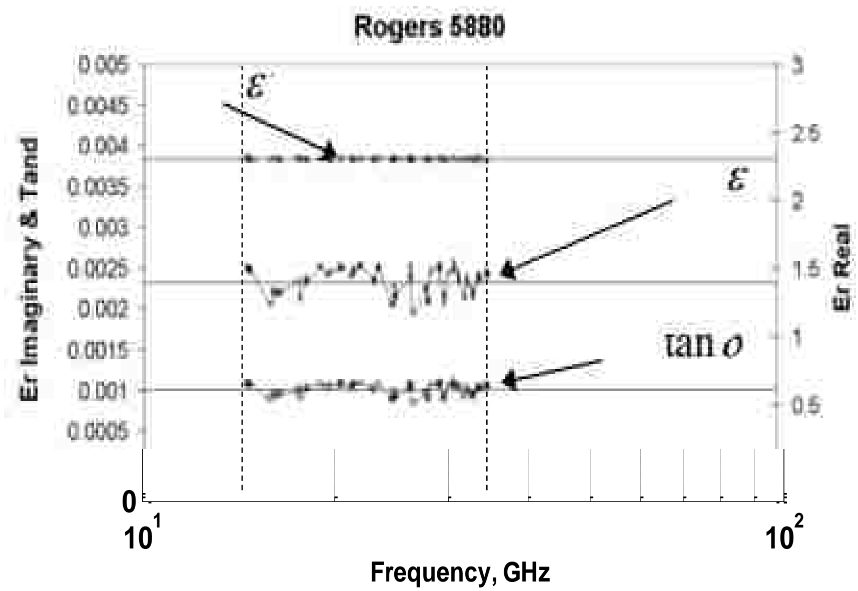

Figure 3.5. Measured of the real and imaginary components of Roger 5880 [33]

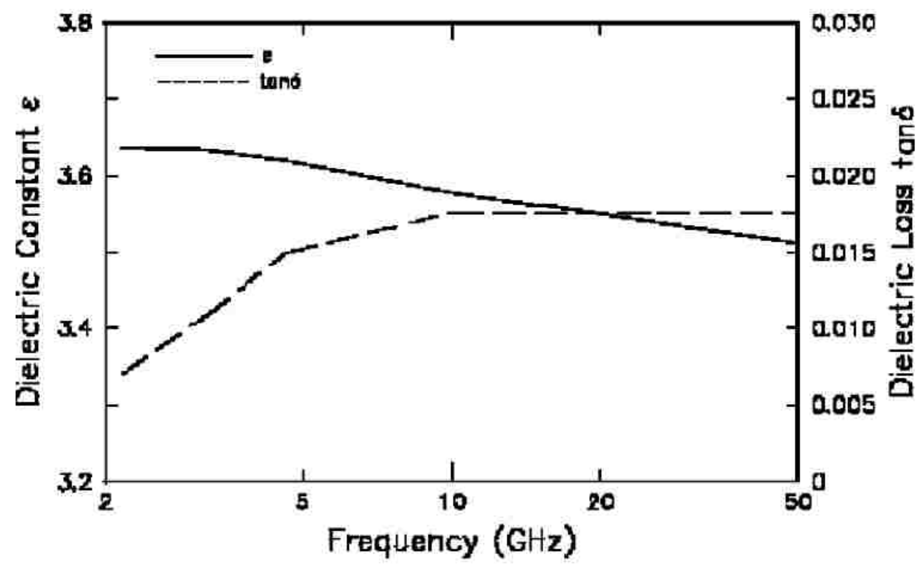

Figure 3.6. DK, DF of bismaleimide triazine (BT) [47]

3.1.2. Motivation and Objective. Generally, these observed effects could not be explained by any existing models as will be demonstrated in the following section, and calls for the development of the alternative approach. Ideally this approach needs to be physics-based, as opposed to phenomenological or behavior modelling. A truly physical approach should involve direct solutions of Maxwell's equations, which might be achieved using one of the commercially available full-wave solvers. There are several challenges that are met when the rough surface is modelled in 3D. The obvious one is that the mesh density (or the number of unknowns) needed to describe the rough surface of a typical PCB conductor is quite high, and might be prohibitive for certain types of solvers. Secondly, the high-frequency 3D solvers do not mesh the inner volume of metal parts, but use boundary conditions to model lossy metals instead. However, the penetration of field into the metal might be comparable to the size of metal protrusions due to the roughness, and boundary conditions might be not adequate in this situation. And thirdly, there are complex chemical compounds that are formed at the interface between the dielectric and metal [34], which might have quite distinctive electrical properties. Currently there is no way to include the effect of these compounds into the 3D model because their properties and the thickness of the layer generally are not known.

Nevertheless, despite these challenges and limitations it was decided to investigate the possibility to model the rough surfaces of the striplines in full-wave primarily to get insights into the physics of the roughness-related attenuation.

3.2. EXISTING MODELS FOR SURFACE ROUGHNESS

Many models for conductor surface roughness are based on representation of roughness profiles by simple shapes. In some models the shapes are placed periodically to simplify the analysis, in others the stochastic methods are employed.

The usual way to estimate the loss due to rough surface is to calculate the correction factor or power loss coefficient. The power loss coefficient is equal to the ratio of the attenuation constant due to conductor loses of a transmission line with rough conductor surfaces to that for the same line with smooth conductor surfaces.

3.2.1. Hammerstad Model. The first model to account for the surface roughness losses was proposed by Morgan in 1949 [35]. In his model, the roughness is

presented as periodic "saw tooth" like structure as shown on Figure 3.7. The assumption behind this theory is that current flows along the edge of the rough surface as it is show on the figure and the additional power losses caused by longer current path. Then he used the finite-difference method to solve a quasi-static eddy-current problem for this structure. As the result the ratio of the power loss dissipated in a conductor with a rough surface $\boldsymbol{\alpha_{rough}}$ to that dissipated in the same but smooth conductor $\boldsymbol{\alpha_{smooth}}$ is calculated.

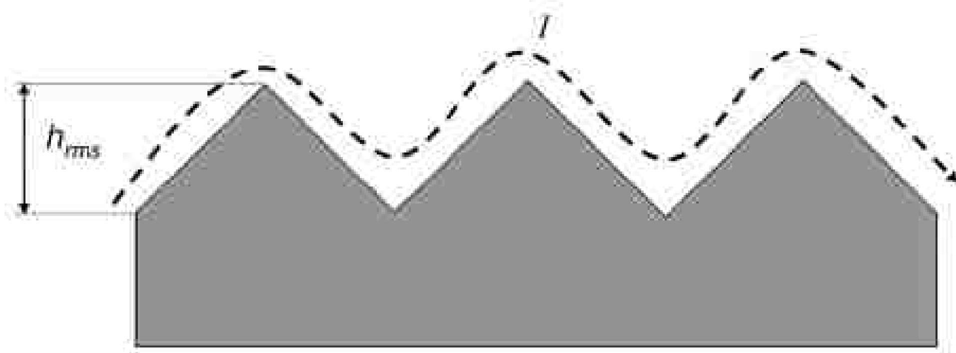

Figure 3.7. Hammersted model for roughness modeling

Later, Hammerstad and Jensen obtained the empirical expression based on Morgan's results for extra loss and used only one parameter, h_{rms} to characterize it [3]:

$$K_s = \frac{\alpha_{rough}}{\alpha_{smooth}} = 1 + \frac{2}{\pi} \cdot arctan\left(1.4\left(\frac{h_{rms}}{\delta}\right)^2\right), \tag{17}$$

where δ is the skin depth. However obtained expression saturates at the value of 2 as it is shown in Figure 3.8 for $h_{rms} = 5.8um$.

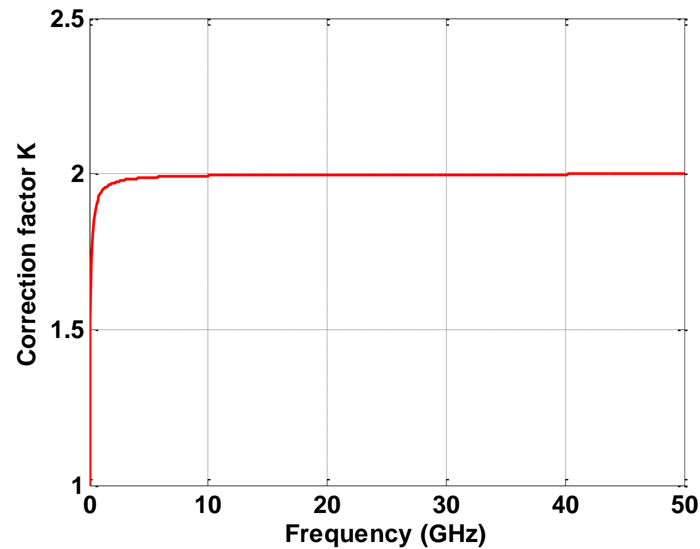

Figure 3.8. Roughness correction factor based on Hammersted model

In practice, the impact of surface roughness can be greater than a factor of 2 which leads to lack of accuracy at high frequencies. The example of loss correction using this method is shown in Figure 3.9.

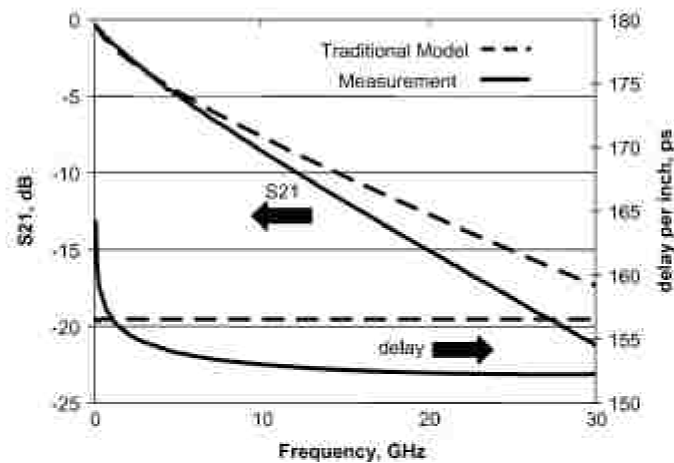

Figure 3.9. Measured and corrected according to Hammersted insertion loss [5]

As it is well seen, the application of Hammersted model is limited to 4-5GHz where it has reasonable accuracy. While this model has been found useful in low frequency speed designs, the modern high-speed circuits require more accurate models.

3.2.2. Hemispherical Model. Hall et al. proposed to model the conductor surface roughness as conductor hemispheres protruding from a at conductor plane [5]. Then, the problem of scattering of a plane wave from the hemispherical protrusion on the flat surface is solved using the method of images. The correction factor is given then as:

$$K_s = \frac{\left(\left|Re\left[\eta\frac{3\pi}{4k^2}(\alpha(1)+\beta(1))\right]\right|+\frac{\mu_0\omega\delta}{4}(A_{tile}-A_{base})\right)}{\frac{\mu_0\omega\delta}{4}A_{tile}} \tag{18}$$

where A_{tile} is the tile area, A_{base} is the base area of the hemispheres, k is wave vector, $\eta = \sqrt{\mu_0/\varepsilon_0\varepsilon'}$ and the first order scattering coefficients are

$$\alpha(1) = -\frac{2j}{3}(kr)^3\left[\frac{1-\frac{\delta}{r}(1+j)}{1+\frac{\delta}{2r}(1+j)}\right] \tag{19}$$

$$\beta(1) = -\frac{2j}{3}(kr)^3\left[\frac{1-\left(\frac{4j}{k^2r\delta}\right)\left(\frac{1}{1-j}\right)}{1+\left(\frac{2j}{k^2r\delta}\right)\left(\frac{1}{1-j}\right)}\right] \tag{20}$$

The parameters for K_s are calculated based on volume equivalent model as:

$$A_{tile} = d_{peaks}^2 \tag{21}$$

$$A_{base} = \pi\left(\frac{b_{base}}{2}\right)^2 \tag{22}$$

$$r = \sqrt[3]{h_{\text{tooth}}\left(\frac{b_{\text{base}}}{2}\right)^2} \tag{23}$$

The meaning of these parameters is illustrated by Figure 3.10.

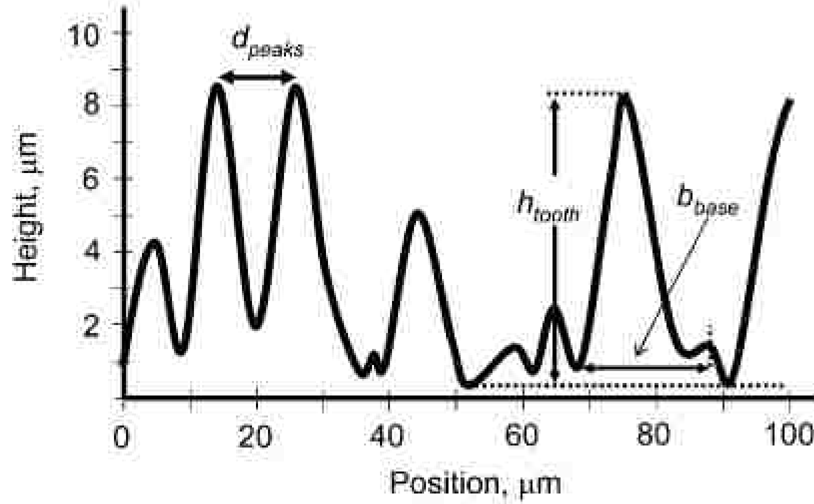

Figure 3.10. Hemispherical model for roughness modeling

An example of applying Eq.(18) with roughness parameters $b_{base} = 9.4um$, $d_{peaks} = 9.4um$, $\varepsilon' = 4$, the correction coefficient in 0 to 50 GHz frequency range is presented in Figure 3.11

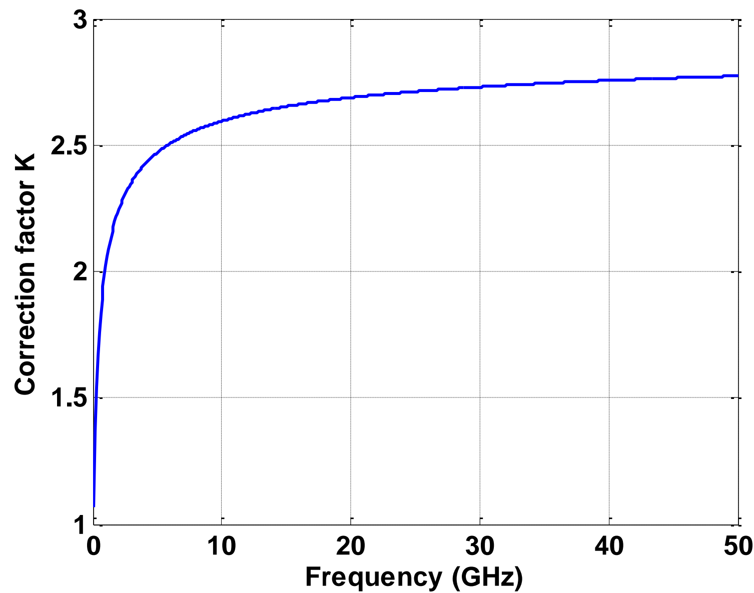

Figure 3.11. Roughness correction factor based on Hemispherical model

Application of this model gives relatively accurate results up to 30 GHz [5] as it is shown on Figure 3.12.

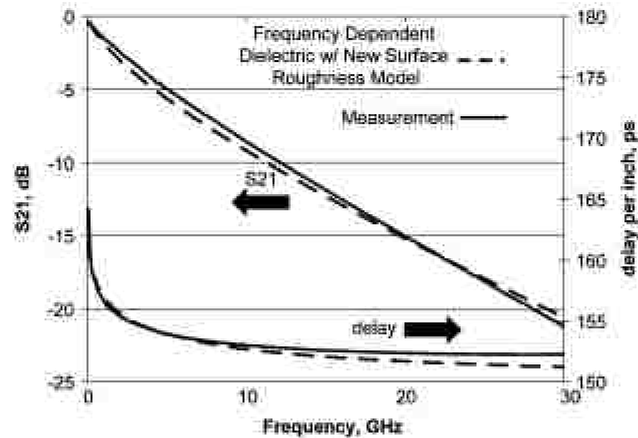

Figure 3.12. Measured and corrected according to Hall insertion loss [5]

Hemispherical model is the most popular today and found implementation in commercial software. It is based on three input parameters and requires three statistical measurements. However, the accurate measurements of base and space between protrusions are required. On the other hand, as can be seen in Figure 3.12, the model typically overestimates loss at low frequencies and underestimates at high ones. And, as the frequency increases past 30 GHz, the underestimation of loss increases.

3.2.3. Snowball Model. In the work of Huray et al. the surface roughness is modeled as a pyramidal stack-up of spherical conductor particles snowballs on a conductor surface [36-37], as shown in Figure 3.13.

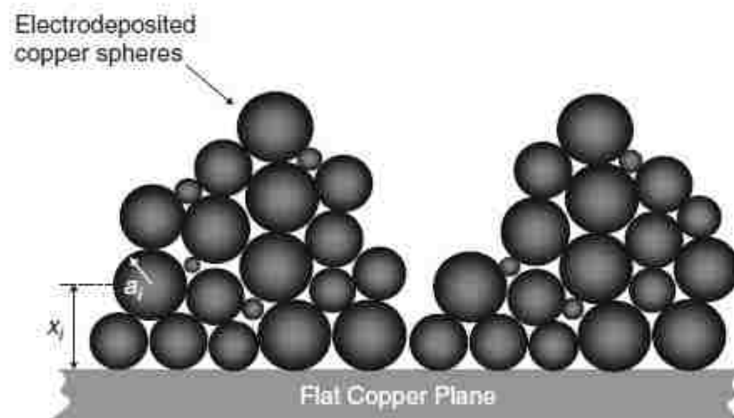

Figure 3.13. Snowballs model for roughness modeling [36]

The problem of scattering and absorption is solved similarly to the hemispherical model but for every sphere. Using the superposition of the sphere losses, the total loss of this structure is derived. As the result the roughness correction factor is written as:

$$K_s = \frac{\frac{\mu_0 \omega \delta}{4} A_{tile} + \sum_{n=1}^{N} Re\left[\eta \frac{3\pi}{2k^2}(\alpha(1)+\beta(1))\right]}{\frac{\mu_0 \omega \delta}{4} A_{tile}} \quad (24)$$

Calculated roughness correction factor is presented on Figure 3.14. Roughness parameters in this example were the same as in previous model and radii of spheres are 0.8μm. Total number of spheres is N=20.

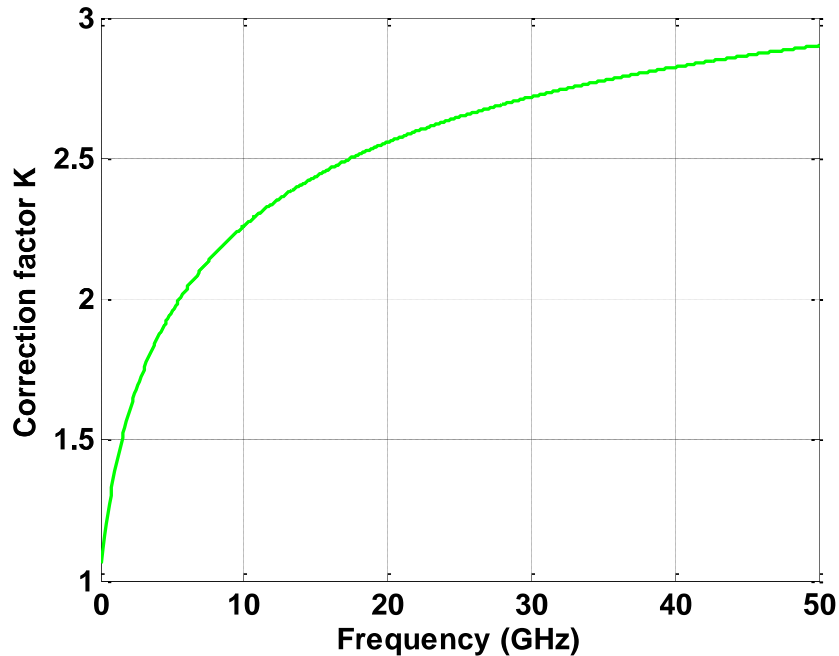

Figure 3.14. Roughness correction factor based on Snowballs model

This model shows the accurate agreement with measurements up to 50GHz but is complicate to use. The application of this model is shown on Figure 3.15.

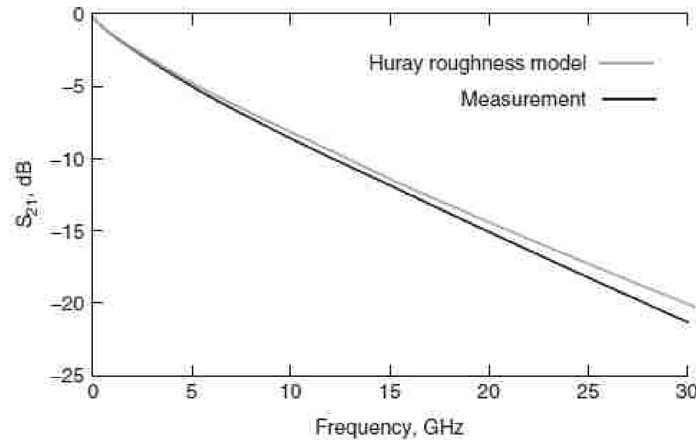

Figure 3.15. Measured and corrected according to Snowball model insertion loss [5]

As can be seen the agreement at lower frequencies is better, but the model also underestimates loss at higher frequency range.

3.2.4. Small Perturbation Method. Tsang et al. conducted more complicated and deep analysis of the surface roughness problem [38-42]. Firstly, they analyzed 2D random rough surfaces based on second order Small Perturbation Method (SPM2) and numerical method of moments (MoM) [42]. Then, they performed calculation of power absorption factor for surface roughness with Gaussian and Exponential correlation functions. Calculations and analysis show that the power absorption enhancement factor depends on three parameters: RMS height, correlation length, and correlation function.

Then this approach has been extended to the analysis of 3D surface roughness where the surface height varies in both horizontal directions [38]. In this work authors derived the closed-form formula of the power absorption enhancement factor based

$$K_s = 1 + \frac{2h^2}{\delta^2} - \frac{4}{\delta}\int_0^{\infty}\int_0^{\infty} dk_x dk_y W(k_x, k_y) Re\left\{\sqrt{\frac{2i}{\delta^2} - k_x^2 - k_y^2}\right\}, \quad (25)$$

where $k_{x,y} = \frac{2\pi n}{L_{x,y}}$ and $W(k_x, k_y)$ is the power spectral density function (PSD).

The example of correction factor calculated using equation (25) is presented on Figure 3.16. Calculation was made for roughness profile having$h_{rms} = 1\ um$, correlation length 2 µm and Gaussian function of PSD.

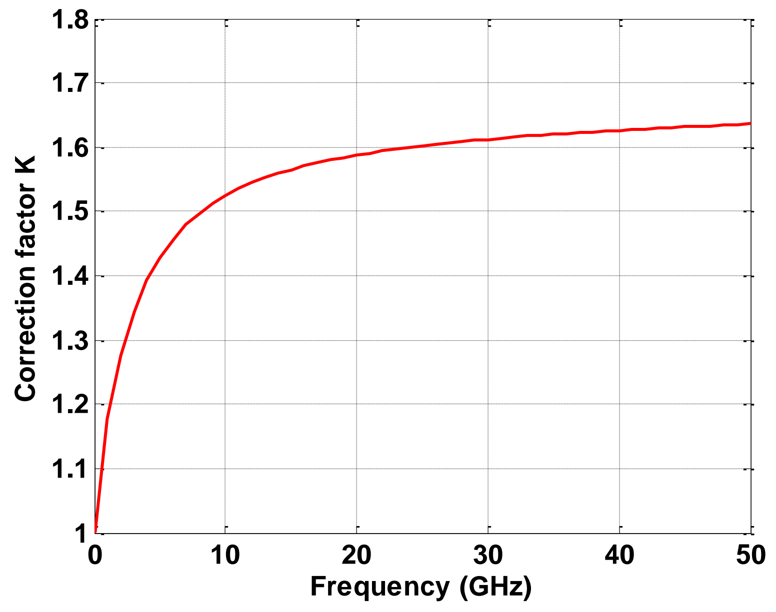

Figure 3.16. Roughness correction factor based on SPM2

The comparison of measured and estimated loss show accurate prediction up to 20 GHz and is presented in Figure 3.17 [39]. However, this method has been tested only for $h_{rms} \leq 1um$ and gives unrealistic correction factor for higher roughness magnitude.

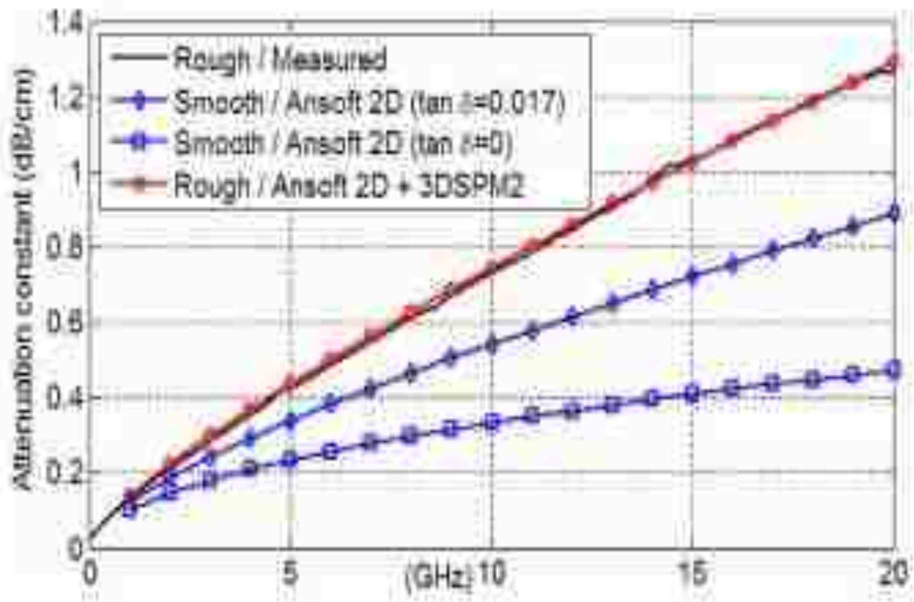

Figure 3.17. Measured and modeled according to SPM2 [39]

3.2.5. Scalar Wave Modeling. Another model based on the stochastic analysis is proposed in the work of Chen and Wong. In their work [43] the rough surface is modeled by parameterized stochastic processes. The method is based on 3D statistical modeling of surface roughness and the numerical solution of scalar wave equation. The extra loss caused by surface roughness is approximated by the energy flux absorbed by the rough surface. The scalar wave modeling (SWM) with the method of moments (MOM) is used to calculate the scattering and absorption of the scalar wave by the rough surface. As the validation of this method the comparison with the SPM2 method was performed (Figure 3.18) but not with the experimental results.

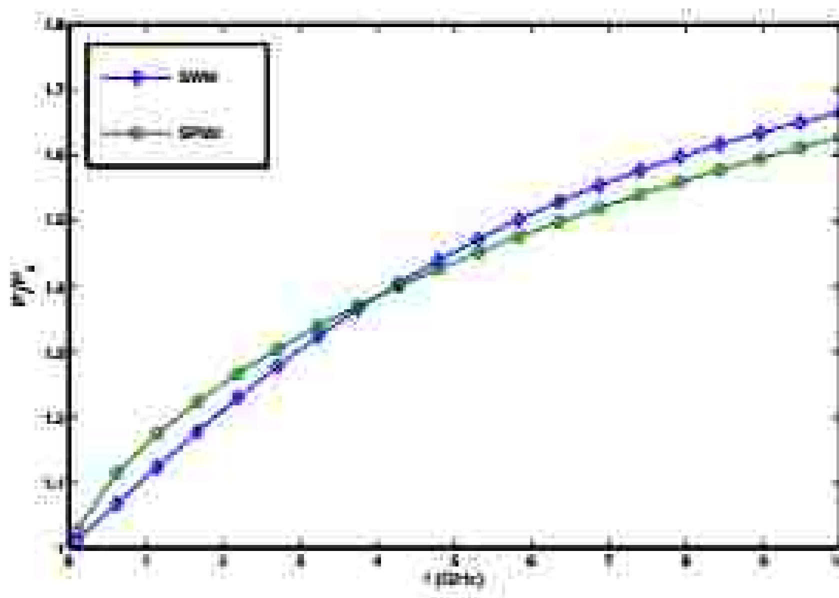

Figure 3.18. Roughness correction factor calculated by SWM vs. SPM2 [43]

Despite the reported advantages of SWM method it was derived based on scalar wave theory instead of EM wave theory

3.2.6. Limitations of Existing Models. As can be seen all of the models reviewed above improve the accuracy of modelling relative to the case when the surface roughness is not taken into account. The accuracy of prediction is different, being the worst for the Hammersted model, and the best for the snowball model. However, none of the existing models is capable to capture the effect of increasing slope of the S21 due to

the roughness that is evident from Figure. 3.3 and 3.4, as the correction factors calculated according to all of them have monotonic second derivative (see Figure 3.8, 3.11, 3.14, 3.16, 3.18). The slope increase effect can be quite strong, adding up to 5 dB loss at 10 GHz (see. Figure 3.4), and definitely requires a closer attention.

3.3. 3D MODEL FOR SURFACE ROUGHNESS

The paper [43] proposes the way to generate a surface resembling the real-word profiles of rough conductors, based on the cross-sectional measurements. We will follow a similar procedure to generate the surfaces that can be automatically imported into CST Microwave Studio.

To generate the random roughness the following steps should be taken:

- Explore the parameters of real roughness. Extract statistical parameters such as probability density function (PDF), Autocorrelation function (ACR), and h_{rms} from the measured roughness profile
- Generate the δ-correlated 2D function (surface) with needed PDF
- Design a filter and filter the δ-correlated function to obtain a surface with needed ACR.
- Import generated surface into CST Microwave studio and perform full wave simulation

3.3.1. Extraction of Roughness Parameters. For the surface roughness characterization the cross section-analysis is essential. To perform the cross-sectional analysis the trace is cut perpendicular to wave propagation direction. For this study several PCB with different foil types have been cut, embedded into a special epoxy compound, polished and the microscopic images of the cross-sections are taken. Prepared samples and microscopic images are presented in Figure 3.19.

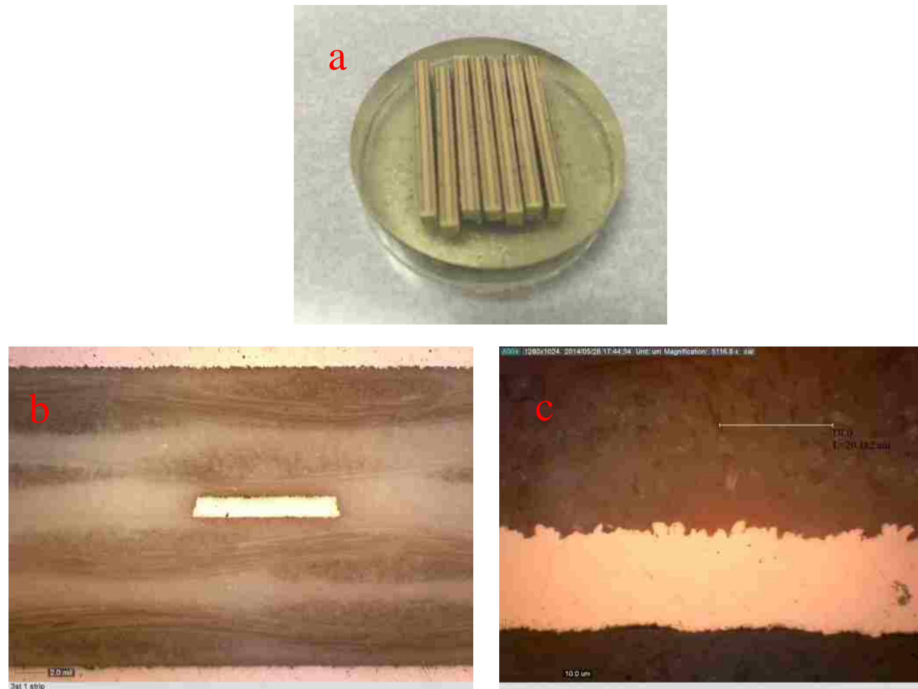

Figure 3.19. Prepared sample for cross section analysis (a), microscopic pictures of stripline (b), close-up picture of the trace (c)

The procedure of image processing for PCB cross section analysis is described in details in [10]. After image processing the binary (black-and white) image of the cross-section is generated. The example of the binary image of the VLP trace is shown in Figure 3.20.

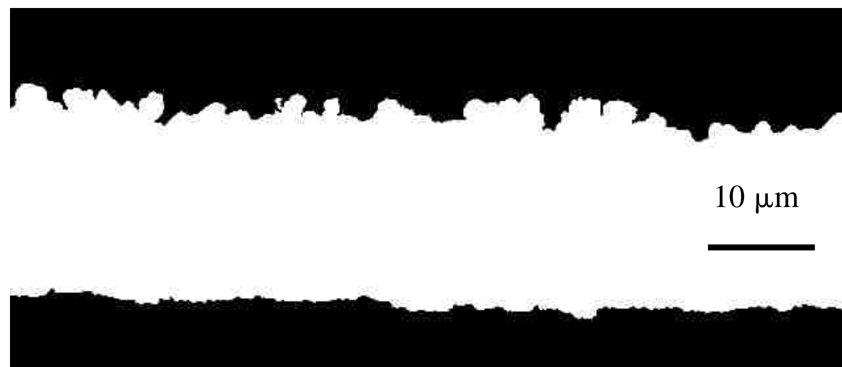

Figure 3.20. Binary image of the cross-section for VLP

The surface roughness profile is extracted directly from the binary images. Roughness profile of the top surface in Figure 3.20 is shown in Figure 3.21 and its autocorrelation function is in Figure 3.22. The histogram of the profile is presented in Figure 3.22.

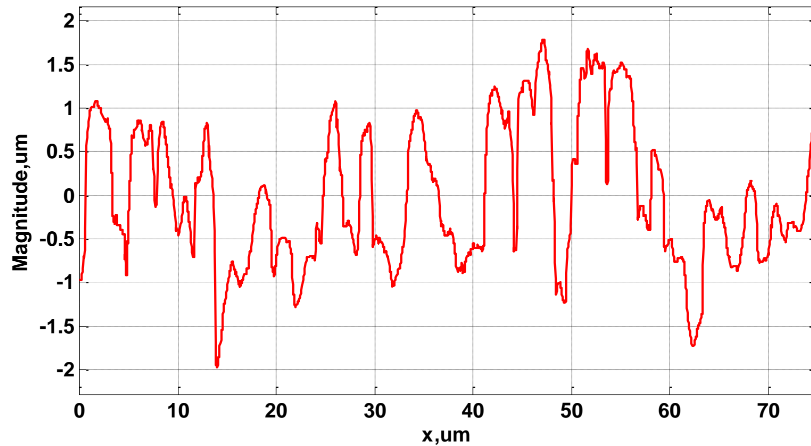

Figure 3.21. Extracted roughness profile of VLP foil (oxide side)

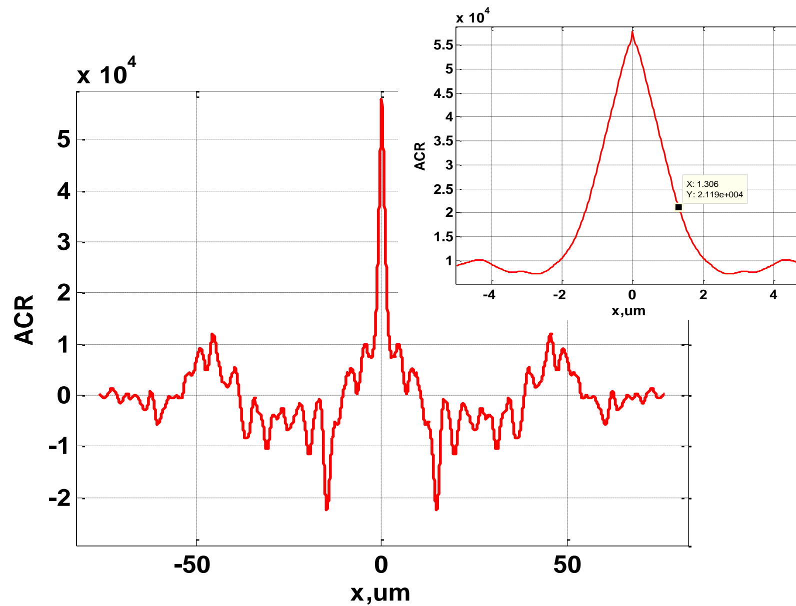

Figure 3.22. Autocorrelation function of the VLP foil roughness profile. Correlation length is indicated by the marker

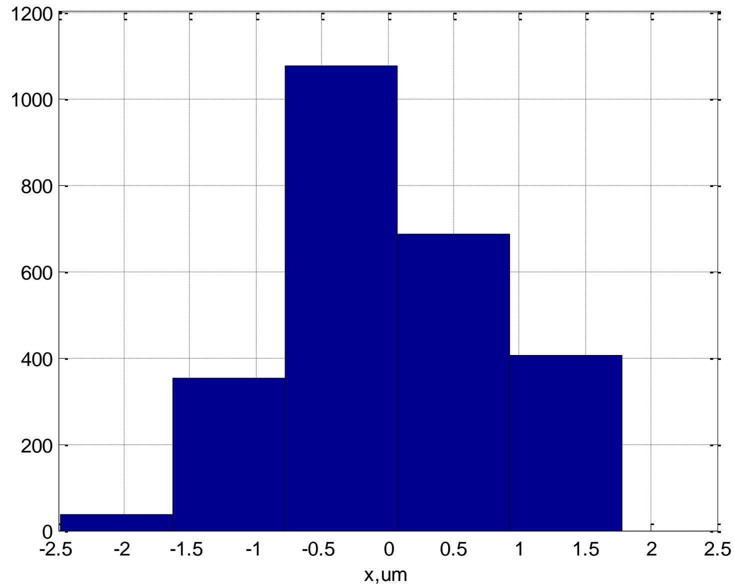

Figure 3.23. Histogram of VLP foil

The correlation length l_{ACR} is defined as the distance where the magnitude of the autocorrelation function decreases e times and is equal to 1.3μm in the case on Figure 3.22. The correlation length can be used to determine the required discretization step, as will be shown later. Measured rms height (according to (6)) of the profile is h_{rms}=0.81 μm. To completely characterize a random function (or a signal) the Probability Density Function (PDF) is needed, however the accurate extraction of it is not possible (as can be seen in Figure 3.23) due to limited number of data samples, and the normal distribution was assumed.

3.3.2. Generation of the 3D Surface. In order to create a random surface, firstly a 2D array filled with δ-correlated random numbers is generated. The numbers have normal distribution with zero mean and standard deviation of 1. The adjustment of the correlation length is achieved by filtering the array by a 2D filter.

Generally the filter might be of any kind if it has a needed frequency response. For instance in [43] a Gaussian 2D filter is used. However, we use 2D finite impulse response (FIR) low pass filter for simplicity of implementation. For the FIR filter of order N, each value of the output sequence $y[n]$ is a weighted sum of the most recent input values and is given as:

$$y[n] = b_0 x[n] + b_1 x[n-1] + \cdots + b_N x[n-N] \tag{26}$$

The internal Matlab function *fir1(N,Wn)* is used to generate the 1D prototype filter. *Wn* is the normalized cut-off frequency which can vary between 0 and 1, where 1 corresponds to the Nyquist frequency. Frequency response of such a filter is presented in Figure 3.24 for *Wn*=0.1 and *N*=4.

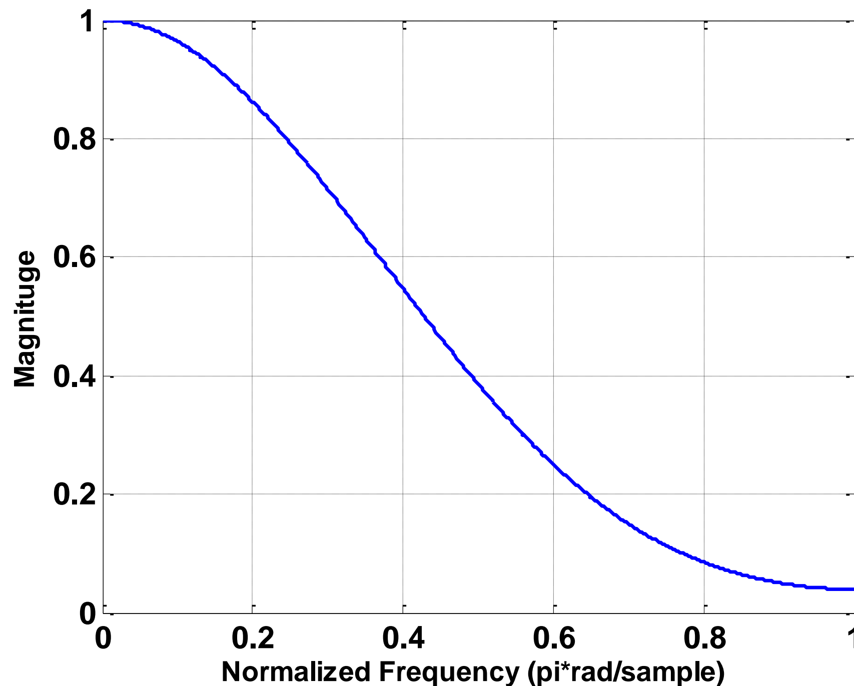

Figure 3.24. Frequency response of a 1D FIR prototype filter

After the 1D prototype filter is generated by the *fir1* functions, the Matlab function *ftrans2(b)* is used to produce the two-dimensional FIR filter that corresponds to the one-dimensional FIR filter.

Examples of frequency response of 2D FIR filters are presented in Figure 3.25 for *N*=4, *Wn*=0.1 and *N*=4, *Wn*=0.8.

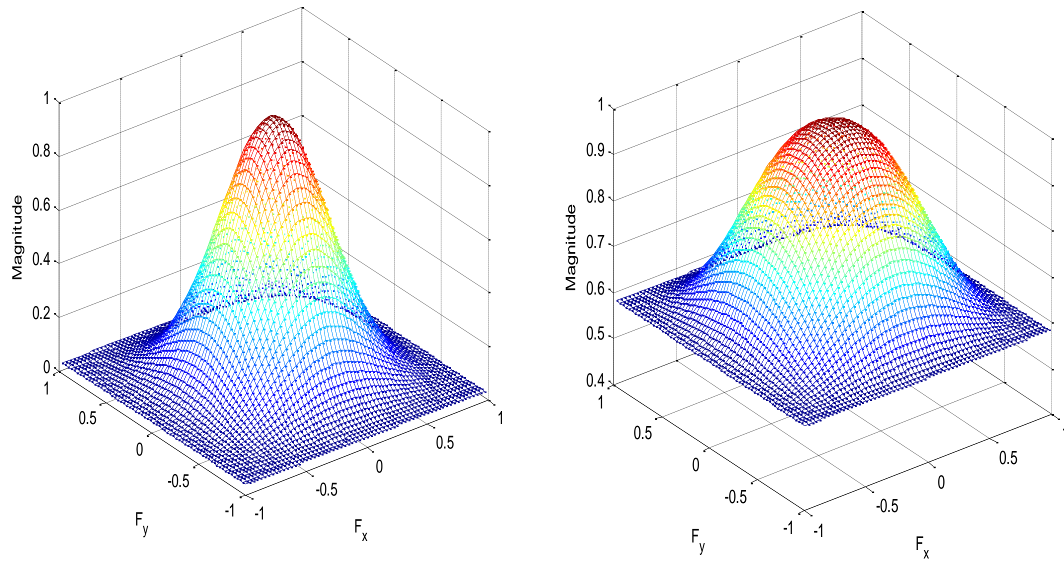

Figure 3.25. Frequency responses for *Wn*=0.1, (right) and *Wn*=0.8 (left). *N*=4 in both cases

The gain of the filter produced by the *ftrans2* function is 1 at zero frequency. In order to obtain the output array with the desired h_{rms}, the output of the filter is multiplied by the gain constant *G*, which is tuned.

Then filtering of 2D δ-correlated array by the 2D FIR filter with the frequency response $H(\omega_1, \omega_2)$ and multiplication by G gives the final rough surface with needed h_{rms}, correlation length and PDF.

Described technique provides opportunity to generate surface of any size and imports it into commercial solvers (technical difficulties of importing are discussed below). The example of generated surface and realistic surface measured by profilometry is presented in Figure 3.26.

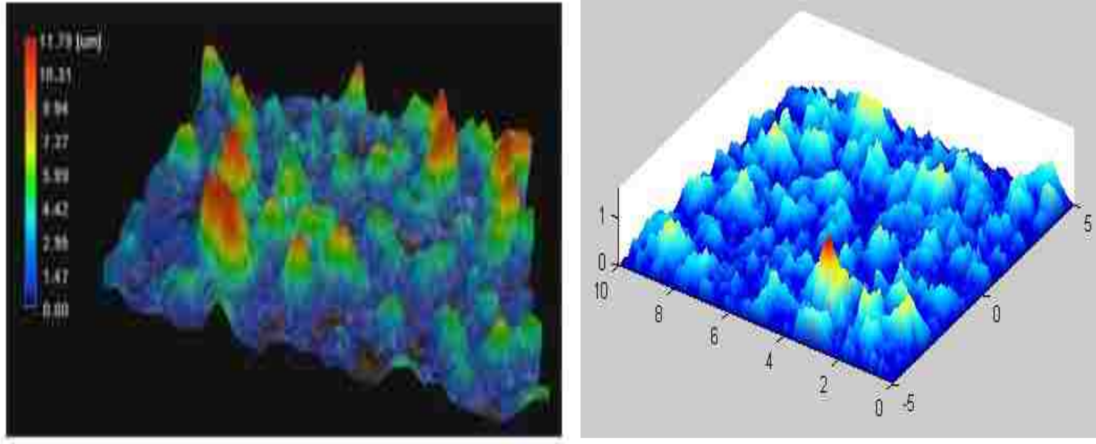

Figure 3.26. Surface roughness profile measured by a profilometer [5] (left) and generated (right)

It is obvious that the autocorrelation function of the sufficiently long δ-correlated sequence of values taken at the interval dx will have triangular shape as illustrated by Figure 3.27.

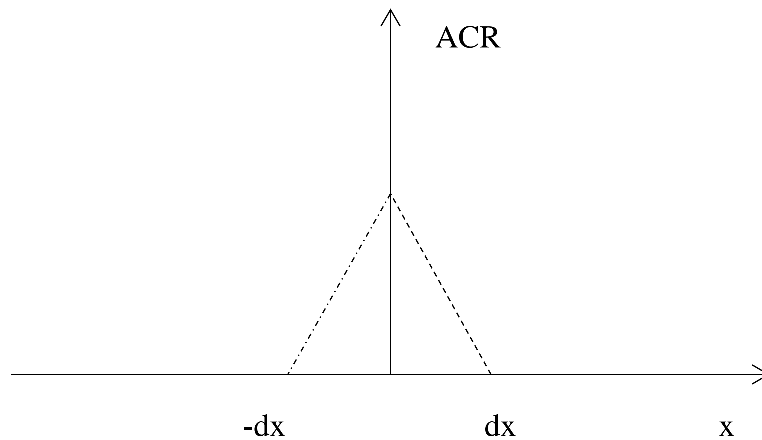

Figure 3.27. Autocorrelation function of δ-correlated sequence

Therefore in order to be able to generate a surface with the required correlation length l_{ACR} the discretization step dx should be smaller than the l_{ACR}. For the example in Figure 3.22, the correlation length is equal to 1.3 μm, which means that dx should be no more than 1.3 μm. However, to produce more realistic profiles the discretization step

should be much smaller than the l_{ACR}. This is illustrated by Figure 3.28 and Figure 3.29 showing the generated profiles along with the measured one for $dx = l_{ACR}$ and $dx = l_{ACR}/10$. Parameters of filter to generate roughness with corresponding discretization steps are given in Table 3.3.

Table 3.3. Filter parameters for two discretization steps

	dx=0.13 µm, (*l/10*)	dx=1.3 µm, (*l*)
Wn	0.03575	0.67787
N	22	4
G	15.646	1.414

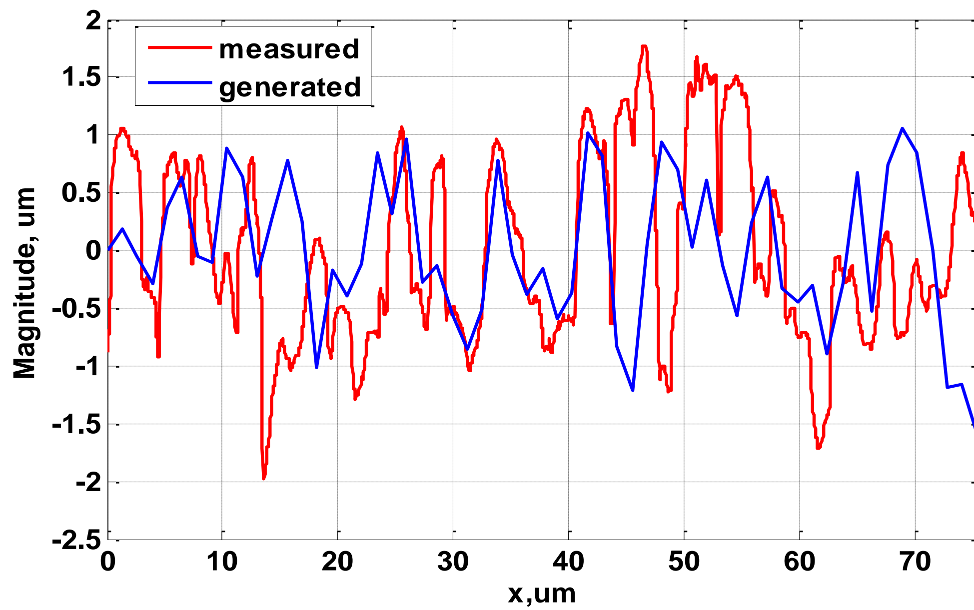

Figure 3.28. Measured and generated profiles of the surface roughness with dx=l_{ACR} (1.3µm)

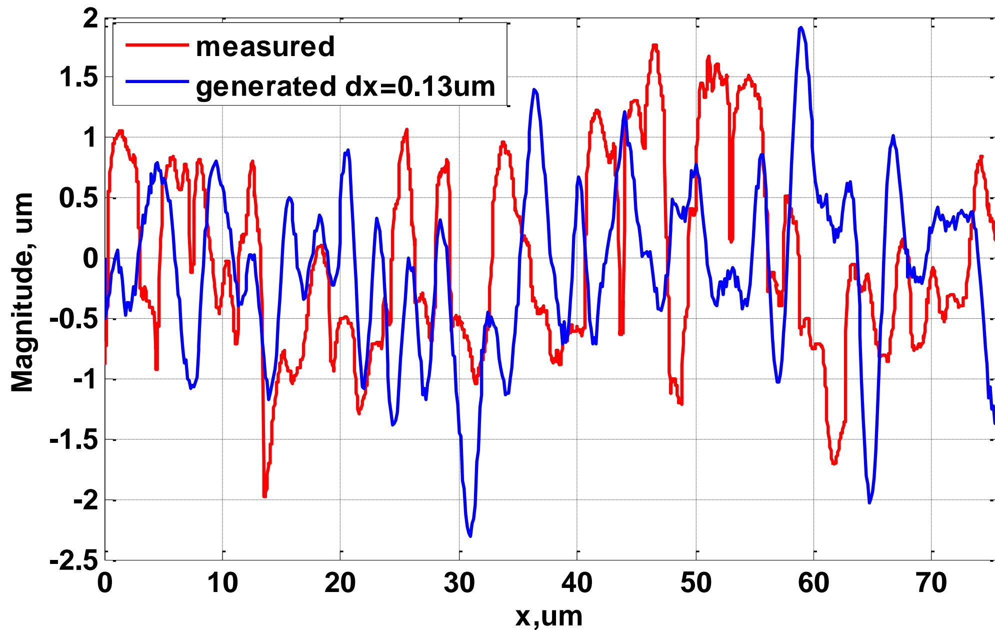

Figure 3.29. Measured and generated profiles of the surface roughness, case dx=$l_{ACR}/10$ (0.13μm)

It can be seen from the figures that good quality of the generated profile can be achieved only if the discretization step is significantly smaller than the correlation length. This is a harsh condition that is difficult to achieve on practice. For example for the 50-mil long and 13 mil wide conductor the number of elements in the array discretized with the step of 0.13 μm (l_{ACR}/10) is $25 \cdot 10^6$, which cannot be handled by CST. The minimum discretization step for the conductor of this size that allowed to successfully generating a functional CST model was 3 μm, which is not enough to adequately describe the realistic profiles with the available computational resources. However, the main goal of this work is to investigate the possibility of creating a full-wave model for surface roughness, and not to model particular roughness profiles. On the other hand, discretization steps below 1μmmight be reached if a more powerful computer is used, or the rough surface is generated directly in CST using VB scripting.

It should be noticed that generated surface cannot be imported into CST directly. In order to import the surface, it needs to be converted to a closed triangulated solid volume by internal Matlab function *sufr2solid.* This function returns generates faces and vertices of a solid body which can be saved as an STL file using the *stlwrite* function

(open-source implementation) [48]. The STL file generated by *stlwrite* can be imported directly to CST or any other 3D solver that supports it.

3.3.3. Surface Roughness Modeling in CST Microwave Studio. Because of the small-scale details of the rough surface the full wave simulations of it require very fine mesh. This leads to extremely high requirements for memory and CPU power which restricts the size of modeled structure. That is why the stripline model needs to be as short as possible. To perform the full-wave simulation the 54mil long 13 mil width stripline was created in CST. To maintain the 50 Ohm characteristic impedance a dielectric with ε=4.3 and tanδ=0.005 (representing a low-loss dielectric like Megtron 6) was used. The cross-section of the signal conductor is 3x13mil, and the distance between the ground planes is 19.5 mil. The vertical boundary conditions were set to magnetic walls to represent infinite span of the ground planes. A solid with the rough surface was generated in Matlab as described above and imported to CST as an additional layer added on top of the smooth central conductor. The length of the rough solid is 50 mil, leaving 2 mil of smooth conductor adjacent to both waveguide ports to allow performing correct excitation of the structure by the ports. The discretization step was set to 4 µm. All conductors are modelled as lossy metal with $\boldsymbol{\sigma = 5.8 \cdot 10^7}$ S/m.

It is important to notice that in order to reach the correlation length close to real roughness the discretization step should be less than 1µm. However, such small step makes it impossible to import generated roughness to CST. The minimum step which allows to run simulation is 2 µm and higher.

The implementation of the stripline structure with rough surface is presented in Figure 3.30 and Figure 3.32. To minimize the mesh requirements two symmetry planes were defined (as shown in Figure 3.31, reducing the total number of mesh cells approximately by 4.

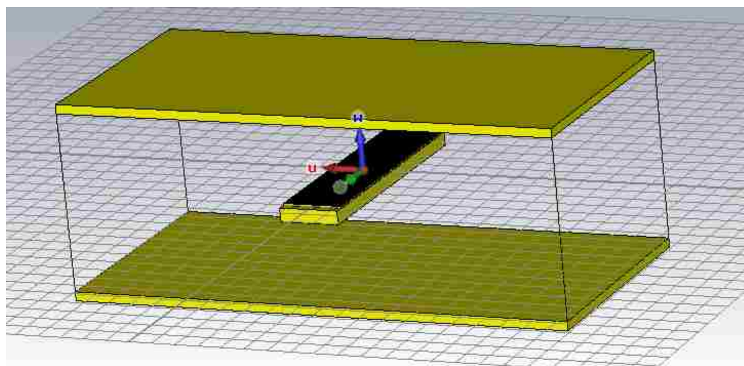

Figure 3.30. Stripline structure to model the surface roughness

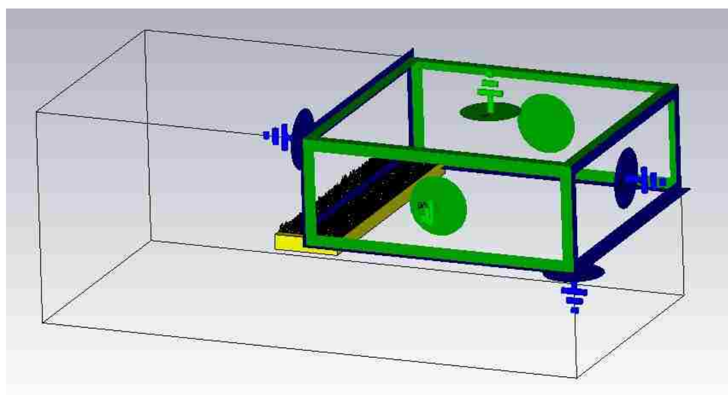

Figure 3.31. Boundary condition and planes of symmetry used for simulation. Blue – magnetic walls, green – electric walls

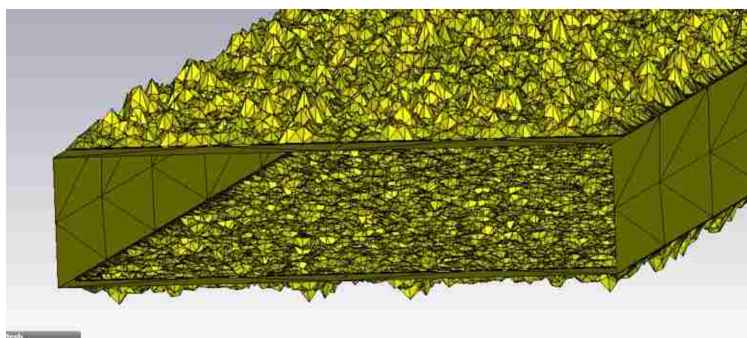

Figure 3.32. Zoom of the end of the trace with surface roughness

The frequency domain FEM solver was chosen for full wave analysis for two reasons. Firstly, the generated rough surface is naturally described by a tetrahedral mesh used in the FEM solver. And, secondly, the transmission coefficients calculated by the FEM solver do not suffer from truncation errors common for the time-domain solver resulting in “ripples” in the obtained curves. The amplitude of these parasitic ripples might be comparable to the effect of roughness itself, making the investigation with the TD solvers virtually impossible.

The efficiency of the model is demonstrated by the Table 3.4, showing the total number of tetrahedrons and simulation time per 1 frequency for different values of *dx*.

Table 3.4. Tetrahedrons and time required for different discretization step

dx, μm	Tetrahedrons	Time per frequency
6.0	41,892	0.9 min
5.0	58.657	1.2 min
4.0	82,551	2.5 min
3.0	210,209	4.3 min

As can be seen, the model is quite efficient, requiring only 4 min per frequency for dx=3 μm. Extrapolating the results in the table the simulation time per frequency for dx=1 μm and dx=0.1 μm can be estimated as 45 min and 5500 min (3.8 days) correspondingly.

Besides the simulation time some time is spent on the importing of the rough surface. This time can be relatively long, reaching 10 min for dx=3 μm, however this operation needs to be performed only once per model.

3.3.4. Results and Discussion. Firstly, several simulations for different discretization steps changing from 3 to 6 μm were performed. The maximum difference in dB(S21) obtained for different discretization step was less than 1% in the entire frequency range, which means that for this particular model the discretization step of 6 μm can be used (which provides short simulation time, allowing to perform parametric sweeps easily) without loss of accuracy.. For further simulations the dx=5 μm was used.

As the next step the simulations were done for different roughness magnitude h_{rms}. In order to do it the rescaling function was used in CST, which allowed

avoiding regenerating the rough surface and reimporting it into CST. This can be done because different realizations of the rough surface produce virtually indistinguishable transmission coefficients as demonstrated by Figure 3.33.

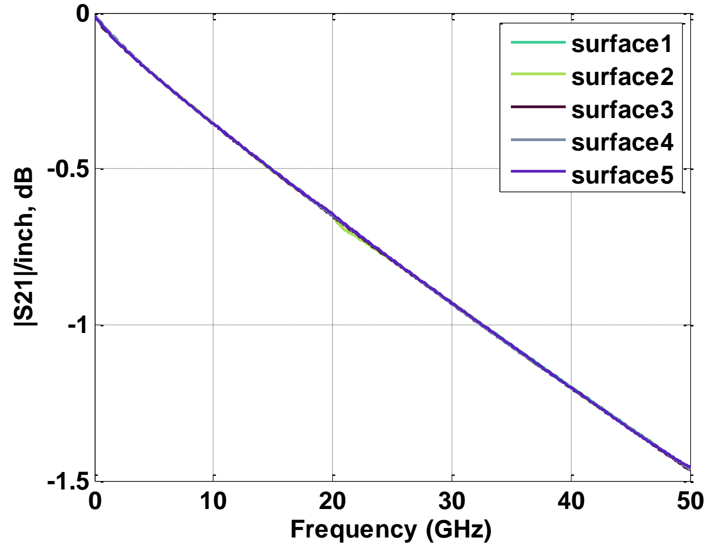

Figure 3.33. Five different realization of surface with the same parameters

The result of the h_{rms} sweep is presented in Figure 3.34 along with the corresponding experimental result from the literature [29].

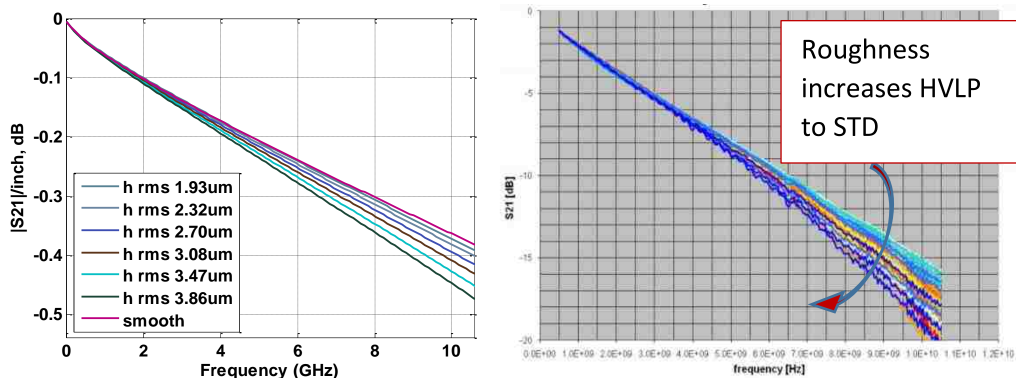

Figure 3.34. Modeled (a) and measured (b) insertion loss for different roughness magnitude up to 10 GHz

At the first glance the obtained results agree very well with the measurements showing the same tendency of increasing slope of the curve.

However, upon closer examination it was noticed that the change of S_{21} slope is due to the change of the reflection coefficient due to the roughness. It can be better understood if the plots of S_{21} (Figure 3.35) and S_{11} (Figure 3.36) are analyzed together up to 50 GHz. It is obvious that the increased insertion loss corresponds to the increased reflection loss, and is actually caused by it, not by the roughness. This effect happens because the line is extremely short and has very small absolute value of insertion loss, such that even very weak reflections on the order of -20 to -40 dB might affect the transmission. To demonstrate it, the transmission loss was corrected by calculating $|S_{21}|^2+|S_{11}|^2$ (this quantity shows the absorption loss in the transmission line). As can be seen from Figure 3.37, the slope of the absorption loss curve remains constant above a certain frequency, however it does depend on the roughness magnitude. This result is very close to the results obtained by all other models reviewed in Section 3.2.

To minimize the effect of reflections, the length of the transmission line was increased by multiplying the rough segment 2, 4 and 8 times. As can be seen from Figures 3.38, 3.39, 3.40, the contribution of the reflection loss to the slope decreases with the length of the line and for the length of 400 mil (x8) the correction for the reflection loss is not needed.

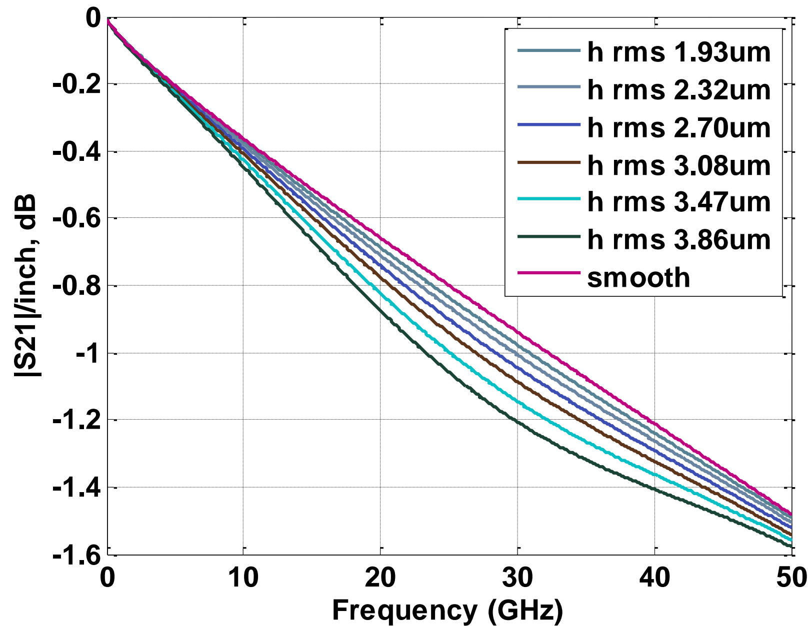

Figure 3.35. Modeled insertion loss for different roughness magnitude up to 50GHz

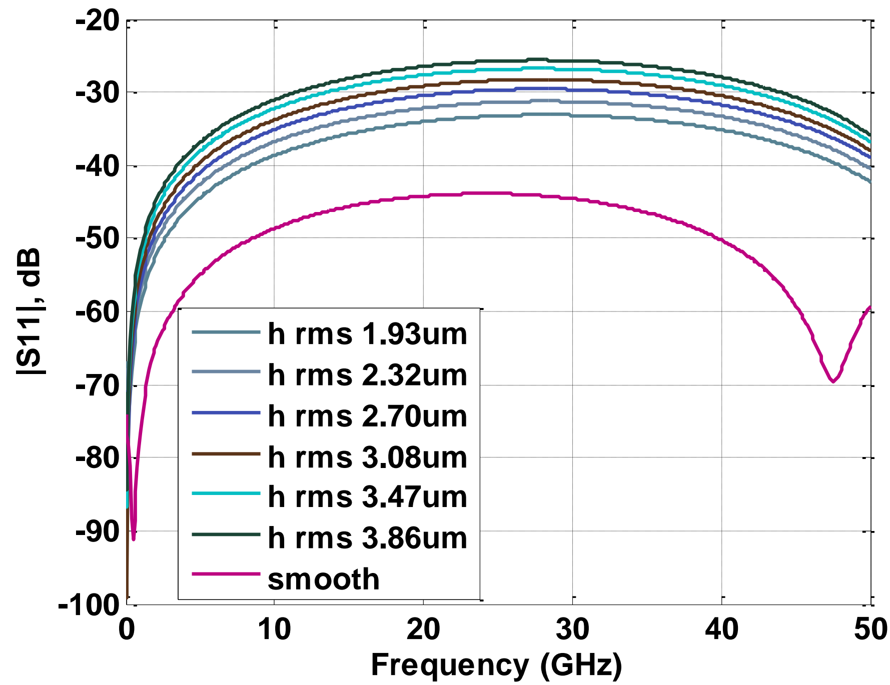

Figure 3.36. Modeled return loss for different roughness magnitude up to 50GHz

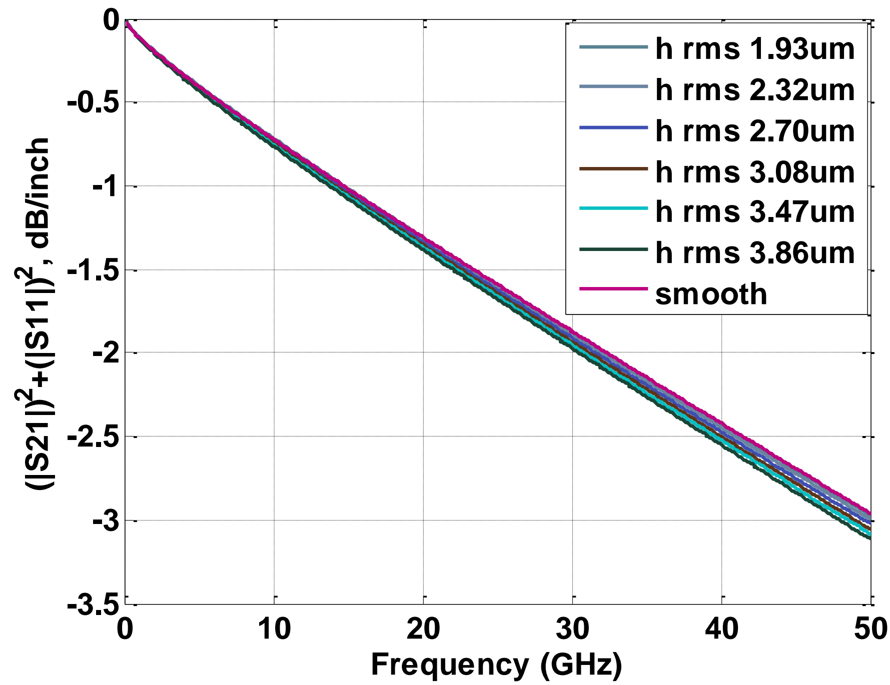

Figure 3.37. Absorption losses for striplines different roughness magnitude up to 50GHz

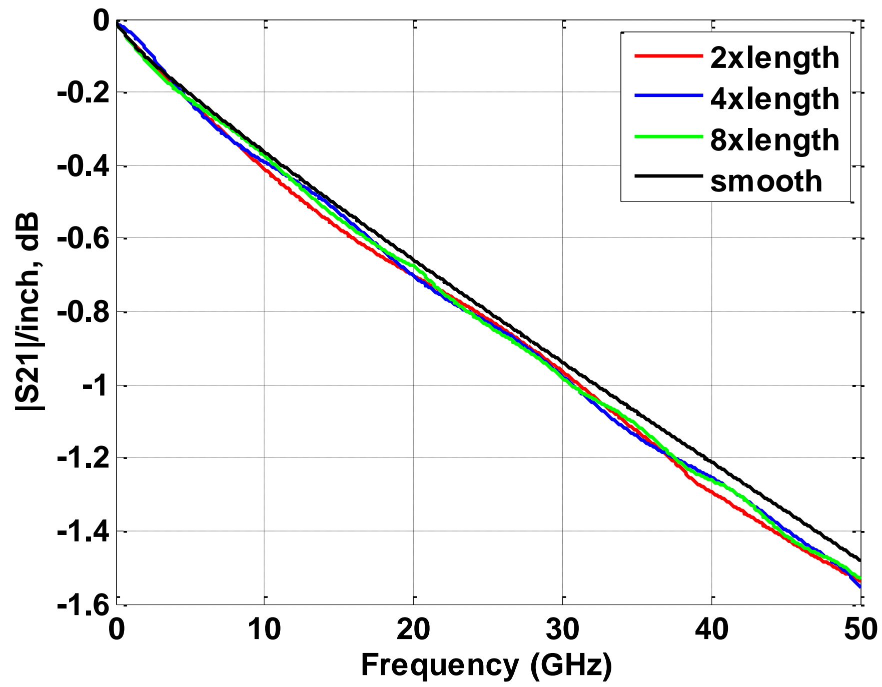

Figure 3.38. Modeled insertion losses for different length of stripline

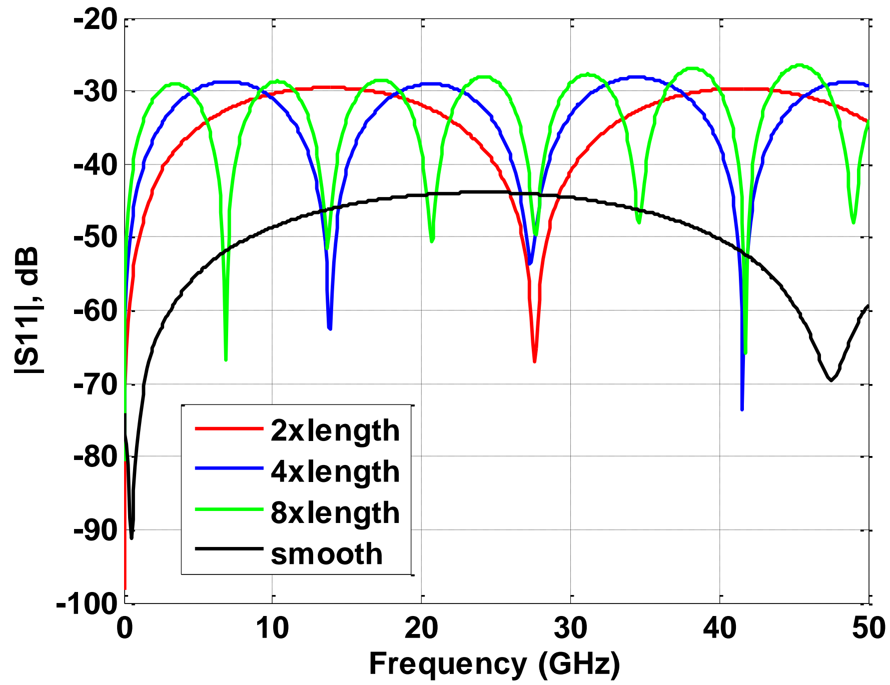

Figure 3.39. Modeled return losses for different length of stripline

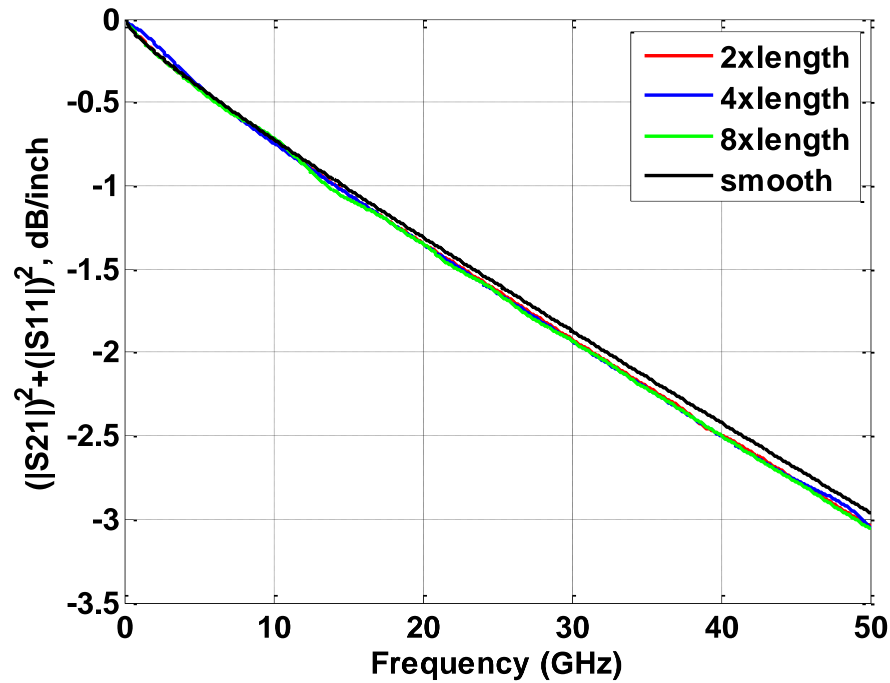

Figure 3.40. Absorption losses for striplines of different length up to 50GHz

The obtained results demonstrate that it is possible to build a realistic full-wave model of a stripline with rough conductors that can be solved easily on workstations, without the need for clusters or super-computers.

At the same time the model failed to reproduce the frequency dependent slope of S_{21} curves observed independently in many measurements. This might indicate that our understanding of physical processes in transmission lines with roughness requires refinement. The proposed full-wave model does not take into account penetration of field into metal, effect of chemical compounds at the interface metal-dielectric, inhomogeneity and anisotropy of the dielectric, which might be responsible for the roughness effect. Potentially, quantum effects might also be relevant.

4. CONCLUSION

The research presented in this thesis is dedicated to conductor-related loss in PCB. There are two sources of conductor losses – skin effect which relates to the finite metal conductivity and the effect of surface roughness. The conductivity of copper and its temperature dependency were investigated experimentally. The effect of surface roughness was modeled using full wave simulation in CST Microwave Studio.

Conductivity of eleven copper types was evaluated using four probe technique at three temperatures. It should be noted that obtained conductivity values are different for all eleven copper types and are lower than nominal values of copper at room temperature. Whereas extracted temperature coefficients converge to values found in literature. Obtained results can be used in simulation related to signal integrity analysis and might prevent the underestimation of actual loss in transmission line. This should be taken into account to better perform the signal integrity analysis.

For surface roughness investigation the set of PCBs with different foil types and trace widths has been measured. Obtained S_{21} curves show expected results - losses increase in rough traces. However, it was also shown that in low loss transmission line, there is unusual behavior of S_{21} – the slope becomes frequency dependent. Literature review confirms this observation, however there was no explanation found of this effect. As an attempt to investigate and understand the nature of this observation, numerous full wave simulations have been performed for generated 3D rough surface. Although this model fails to predict frequency dependent slope of S_{21} curves, the methodology proposed in this work for 3D rough surface generation compatible with EM solvers can be used for further roughness effect investigation.

BIBLIOGRAPHY

[1] E.Bogatin, Signal Integrity- simplified, Upper Saddle River, NJ, Pearson Education Inc., 2004.

[2] S. Hall and H. Heck, Advanced Signal Integrity for High-Speed Digital Designs. New York, NY, USA: Wiley, 2009.

[3] O. Jensen and E. Hammerstand, "Accurate models for microstrip computer-aided design," IEEE MTT-S Digest, pp. 407-409, 1980.

[4] G. Brist, S. Clouser and T. Liang, "Non-classical conductor losses due to copper foil roughness and treatment," ECW 10 Conf. at IPC Circuits Designers Summit, pp. S19-2-1-S19-2-1-11, 2005.

[5] S. Hall, S. Pytel, P. Huray, D. Hua, A. Moonshiram, G. Brist, and E. Sijercic, "Multigigahertz causal transmission line modeling methodology using a 3-D hemispherical surface roughness approach," Microwave Theory and Techniques, IEEE Transactions on, vol. 55, no. 12, pp. 2614-2624, Dec 2007.

[6] D. M. Pozar, Microwave Engineering , 2nd ed., Wiley, New York, NY, 1998.

[7] R. A. Matula, "Electrical Resistivity of Copper, gold, Palladium, and Silver," J. Phys. Chem. Ref.Data, Vol.8, No.4, 1979.

[8] S. Hinaga, M.Y. Koledintseva, "Thermal Effects on PCB Laminate Material Dielectric Constant and Disipation Factor," Techn. Conf. IPC Expo/APEX 2010, Las Vegas, April 5-8, 2010.

[9] "Copper-Foils-for-High-Frequency-Circuit-Materials", available at https://www.rogerscorp.com/docµments/749/acs/Copper-Foils-for-High-Frequency-Circuit-Materials.pdf.

[10] S. De, A. Gafarov, M. Koledintseva, S. Hinaga, R. J. Stanley, J. Drewniak, "Semi-Automatic Copper Foil Surface Roughness Detection from PCB Microsection Images", 2012 IEEE International Symposium on Electromagnetic Compatibility (EMC).

[11] Y. Shlepnev, "Dielectric and Conductor Roughness Models Identification for Successful PCB and Packaging Interconnect Design up to 50 GHz," The PCB Design Magazine 02/2014; 2014(2):12-28.

[12] Gary Brist, Stephen Hall, Sidney Clouser, & Tao Liang "Non-Classical Conductr Losses Due to copper Foil Roughness and Treatment," ECWC 10 Conference at IPC Printed Circuits Expo, SMEMA Council APEX and Designers Summit 05.

[13] Lazarus Weiner, Premo Chiotti, H. A. Wilhelm, "Temperature dependence of electrical resistivity of metals," United States Atomic Energy Commission, Technical Information Service, 1952.

[14] Lorenz. L., "III. Concerning the Conductivity of Metals for Heat and Electricity," Ann. Phys. 3, 13, 582-606, 1881.

[15] Jaeger, W., and Diesselhorst, H., "Thermal Conductivity, Electrical Conductivity, Heat Capacity, and Thermoelectric Power of Several Metals," Wiss. Abh. Phys.-Tech. Reichsanst. 3, 269-425, 1900.

[16] J. H. Dellinger, "The Temperature Coefficient of Resistance of Copper," Bulletin of the Bureau of Standards, Vol.7, No.1, 1900.

[17] Niccolai, G., "Electrical Resistivity of Metals Between Very High and Very Low Temperatures," Phys. Z. 9(11), 367-72, 1908.

[18] Northrup E.F., "Resistivity of Copper in Temperature Range 20C to 1450C," J. Franklin Inst. 177(1), 1-21, 1914.

[19] S. W. Stratton "Copper wire tables," United States. National Bureau of Standards 3d Ed., No.31, Oct. 1, 1914.

[20] Gruneisen, E., and Goens, E., "Investigation of Metal Crystals. V. electrical and Thermal Conductivity of Single and Polycrystalline Metals of Regular Systems," Z. Phys. 44, 615-42, 1927.

[21] Laubitz, M. J., "Transport Properties of Pure Metals at high Temperatures. I. Copper," Can. J. Phys. 45(11), 3677-96, 1967.

[22] Smits, F. M., "Measurements of Sheet Resistivity with the Four-Point Probe," Bell Syst Tech J.1958;37:371.

[23] Valdes, L., "Resistivity Measurements on Germanium for Transistors", Proc. IRE 42 420, 1954.

[24] "Evaluation of measurement data — Guide to the expression of uncertainty in measurement," Joint Committee for Guides in Metrology (JCGM) 100:2008.

[25] Taylor, John. An Introduction to Error Analysis, 2nd. ed. University Science Books: Sausalito, 1997.

[26] Baird, D.C. Experimentation: An Introduction to Measurement Theory and Experiment Design, 3rd. ed. Prentice Hall: Englewood Cliffs, 1995.

[27] Lichten, William. Data and Error Analysis., 2nd. ed. Prentice Hall: Upper Saddle River, NJ, 1999.

[28] Bevington, Phillip and Robinson, D. Data Reduction and Error Analysis for the Physical Sciences, 2nd. ed. McGraw-Hill: New York, 1991.

[29] A. Ippich, "A Designs Experiment for the Influence of Copper Foils on Impedance, DC Line Resistance and Insertion Loss," IPC APEX Expo 2012.

[30] Lee, B "The Impact of Inner layer Copper Foil Roughness on Signal Integrity", Printed Circuit Design and Fab, April 2007.

[31] Briest, G. and Hall, S. "Non-Classical Conductor Losses due to Copper Foil Roughness and Treatment", IPC Printed Circuit Expo 2005.

[32] Y. Shlepnev, A. Neves, T. Dogostino, S. McMorrow, "Measurement-Assisted Electromagnetic Extraction of Interconnect Parameters on Low- Cost FR-4 boards for 6-20 Gb/sec Applications "DesignCon 2009.

[33] S. G. Pytel, G. Barnes, D. Hua, A. Moonshiram, G. Brist, R. Mellitz, S. Hall, and P. G. Huray, "Dielectric modeling, characterization, and validation up to 40 GHz," presented at the 11th Signal Propag. on Interconnects Workshop, Genoa, Italy, May 13–16, 2007.

[34] S. Hinaga, M., Koledintseva, P. K. Reddy Anmula, & J. L Drewniak, "Effect of conductor surface roughness upon measured loss and extracted values of PCB laminate material dissipation factor," IPC APEX Expo 2009 Conference, La Vegas, March 2009.

[35] S. P. Morgan, "Effect of surface roughness on eddy current losses at microwave frequencies," Journal of Applied Physics, vol. 20, no. 4, pp. 352-362, Apr 1949.

[36] P. Huray, S. Hall, S. Pytel, F. Oluwafemi, R. Mellitz, D. Hua, and P. Ye, "Fundamentals of a 3-D snowball model for surface roughness power losses," in Signal Propagation on Interconnects, 2007. SPI 2007. IEEE Workshop on, May 2007, pp. 121-124.

[37] P. G. Huray, O. Oluwafemi, J. Loyer, E. Bogatin, and X. Ye, "Impact of copper surface texture on loss: A model that works," DesignCon 2010 Proceedings, 2010.

[38] L. Tsang, X. Gu, and H. Braunisch, "Effects of random rough surface on absorption by conductors at microwave frequencies," Microwave and Wireless Components Letters, IEEE, vol. 16, no. 4, pp. 221-223, April 2006.

[39] X. Gu, L. Tsang, and H. Braunisch, "Estimation of roughness-induced power absorption from measured surface profile data," Microwave and Wireless Components Letters, IEEE, vol. 17, no. 7, pp. 486-488, July 2007.

[40] H. Braunisch, X. Gu, A. Camacho-Bragado, and L. Tsang, "On-chip rough-metal-surface propagation loss modeling and correlation with measurements," in Electronic Components and Technology Conference, 2007. ECTC '07. Proceedings. 57th, May 2007, pp. 785-791.

[41] L. Tsang, X. Gu, and H. Braunisch, "Effects of random rough surface on absorption by conductors at microwave frequencies," IEEE Microw. Wireless Compon. Lett., vol. 16, no. 4, pp. 221–223, Apr. 2006.

[42] X. Gu, L. Tsang, H. Braunisch, and P. Xu, "Modeling absorption of rough interface between dielectric and conductive medium," Microw. Opt. Technol. Lett., vol. 49, pp. 7–13, Jan. 2007.

[43] Q. Chen and N. Wong, "New Simulation Methodology of 3D Surface Roughness Loss for Interconnects" Design, Automation and Test in Europe, DATE 2009, Nice, France, April 20-24, 2009.

[44] "In Intelligent Signal Processing and Communications, 2006. ISPACS '06. International Symposium on, Dec 2006, pp. 411-414.

[45] Advanced Design System, Retrieved from http://www.keysight.com/en/pc-1297113/advanced-design-system-ads?cc=US&lc=eng.

[46] J. A. Marshall, "Measuring Copper Surface Roughness for High Speed Applications," Retrieved from http://www.circuitinsight.com/pdf/measuring_copper_surface_roughness_ipc.pdf.

[47] A. Deutsch, e.t. "Extraction of $\varepsilon_r(f)$and $\tan\delta(f)$ for Printed Circuit Board Insulators Up to 30 GHz Using the Short-Pulse Propagation Technique," IEEE Transactions on Advanced Packaging, vol.28, no.1, Feb. 2005.

[48] Export a variety of inputs (patch, surface) to an STL triangular mesh (30 Jul 2008). Retrieved from http://www.mathworks.com/matlabcentral/fileexchange/20922-stlwrite-filename--varargin-.

VITA

Mr. Oleg Kashurkin was born in Russia. He received his State Specialist Diploma (equivalent MS) degree in Physics with specialization in Radiophysics and Electronics from Department of Science, Peoples Friendship University of Russia in June 2006.

In 2008-2011 he worked as Sr. Engineer in Laboratory of Microwave Composite at Institute for Theoretical and Applied Electromagnetics, Russian Academy of Science.

In August 2013 he joined the EMC Laboratory of Missouri University of Science and Technology as the graduate student and has been working as a research assistant. In May 2016 he received his Master Degree in Electrical Engineering from Missouri University of Science and Technology.